DOCUMENT 3
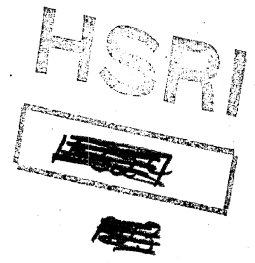

A HYBRID COMPUTER MODEL

OF TIRE SHEAR FORCE GENERATION

Hans B. Pacejka

December 1971

A Study Sponsored by

the Automobile Manufacturers Association

LIST OF CONTENTS

1. INTRODUCTION

In this report a technique will be discussed which offers

hope for investigating and simulating tire models which can be

considerably more complex than existing models used in connection

with the study of tire shear force generation. The simulation of

the behavior of two different tire models will be discussed in this

report. Reference [1] gives a concise description of this investi-

gation. As often is the case, tackling a problem becomes easier

when using a method which comes closer to the way nature "solves"

the problem. Frank (Ref. [2]) was the first to recognize the

potentials of following a material element of the tire in its motion

through the contact range and the rest of the tire circumference.

The material element he elected to follow was part of the beam

or string. The differential equation governing this motion has an

unstable solution and a special iterative method was devised for

obtaining a solution that fits the boundary conditions. Frank

restricted himself to pure sideslip (no braking or driving force)

and a constant friction coefficient. In his doctoral thesis,

Willumeit proposed following a certain element of tread during

its motion through the contact patch (Ref. [3]). The base of the

elastic element is assumed to move along a straight line and the

tire model that is assumed is essentially a brush type with rigid

carcass. The friction coefficient was considered in Willumeit's

study to vary with sliding speed and both longitudinal and lateral

slip were taken into account. The resulting equations of motion

were solved by means of a digital computer.

The "tread element following" method has been adopted in modified form for our investigation and it has been extended to a model exhibiting carcass elasticity. The hybrid computer appears to be the computational device best suited to solve the problem. In addition to steady-state motions, transient motions may be considered.

First, a relatively simple model which is identical to the model developed in Reference [4] and which will be designated as the brush type model, will be considered. In the present study the pressure distribution and friction coefficient can be chosen according to experimental findings. By proper selection of parameter values the model is expected to give satisfactory results. These parameters may be taken as functions of vertical load, speed of travel, and road contamination state.

This relatively simple model is thought to be useful mainly in connection with the simulation of the motion of a complete vehicle. The relatively slowly varying motions of the automobile may be calculated by the digital computer when the hybrid configuration is used. The rapid motions of the tread element when running through the contact area is simulated by the analog computer. Some of the functions used in the latter simulation may also be computed by the digital computer. For example the vertical pressure distribution over the contact length and stiffnesses which vary with vertical load and thus with load transfer. When the speed of travel varies considerably during one simulation run, also the coefficient of friction function would be updated during that run.

The second model to be discussed is particularly useful for the investigation of tire response as influenced by tire structural

parameters. The effect of such parameters as carcass geometry and material properties is represented by an influence or Green function. It will also be demonstrated that the response to camber angle can be simulated by this model in a natural manner. Moreover, the introduction of carcass compliance creates the possibility of examining the response to time-varying wheel-axle motion inputs. The wavelength should be chosen large with respect to the contract length. By increasing the number of tread elements which are followed simultaneously during one passage and by considering more than one row of tread elements each exhibiting different contact lengths and pressure distributions (functions of vertical load, slip angle, camber angle, etc.), the model approaches the nearly perfect representation of the real tire. Note, however, that mass and hysteresis of the tire body has not been included. High frequency motions are as yet disregarded. The approximate theory of high frequency response developed in Reference [5] may give an indication in which direction the model must be modified in order to cover also this aspect of tire response.

2. BRUSH-TYPE TIRE MODEL

The first model to be treated consists of a rigid carcass provided with a row of elastic tread elements which contact the road surface over the length where the vertical pressure possesses a positive value. Of the large number of elements present in the contact range only one will be followed during its passage through the contact patch. For steady-state motions the deflections and shear forces at a x-coordinate (i.e., at a certain distance behind or ahead of the vertical plane through the wheel-axle) do not change with time. Consequently, the integral of shear forces encountered by one element when running through the contact patch produces the total forces and moment acting from ground to tire. Under the influence of longitudinal and lateral slip, the element (Figure 1) which may show different stiffnesses in lateral (y) and longitudinal (x) directions, undergoes a complex variation of deflections. The decaying friction coefficient function (Figure 2) causes the motion to become unstable. In practice, this is reflected in the often observed slip-stick phenomenon. The model's tread element exhibits both mass (necessary for an oscillating motion) and damping (for stabilizing the motion). For the sake of simplicity, it is assumed that μ is a continuous function of sliding speed, V_s, and approaches zero when $V_s \rightarrow 0$.

The base point, B, of the elastic element which is the point where the element is attached to the carcass (Figure 3), moves in a plane parallel to the wheel center plane. The plane may be offset with respect to the wheel center plane by the amount $\tilde{v}_c$ corresponding to a lateral uniform deflection of the carcass. In addition, a

4

longitudinal shift $\tilde{u}_c$ of the contact length may occur due to a driving or braking force. The influence of these shifts is felt in the resulting aligning torque (about the vertical axis through the wheel center). These uniform carcass deformations will be held constant during each run of the element through the contact patch and updated at the end of each run. Only an effective fraction of the carcass deflection $(\tilde{u}_c, \tilde{v}_c)$ may be taken into account due to the fact that the center of vertical pressure is not shifted over the same distance.
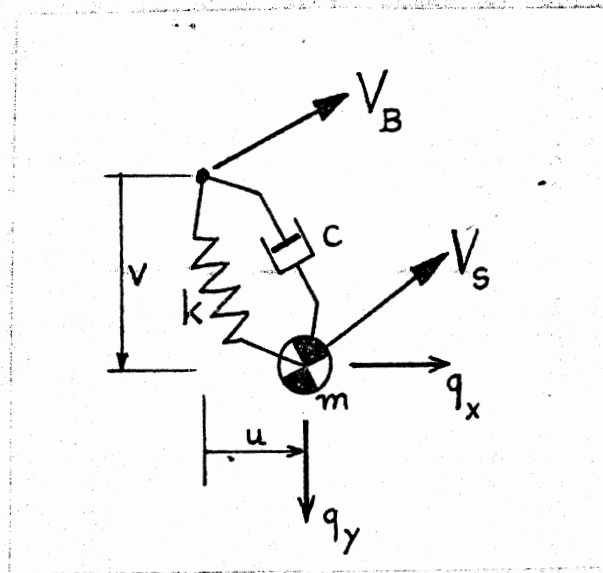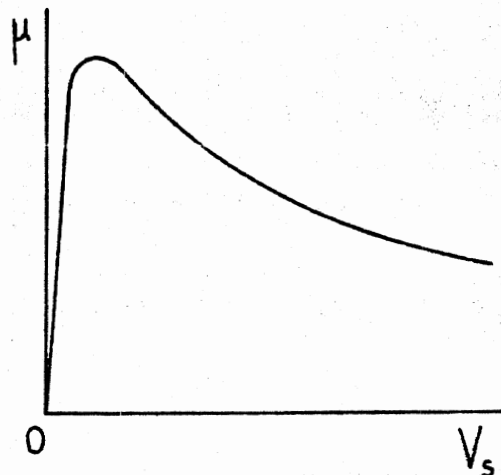

Figure 1. Tread Element.

Figure 2. Coefficient of Friction.

5

Figure 3. The Rigid Carcass (Brush-Type) Tire Model

The center of the wheel has a speed V. Slip angle α indicates the angle between speed direction and (vertical) wheel center plane. We have a lateral speed, V_y, which is equal to the lateral slip or creep speed, V_{cy}:

$$V_y = V_{cy} = V \sin \alpha \qquad (1)$$

The longitudinal speed of the wheel center becomes:

6

$$V_x = V \cos \alpha \tag{2}$$

The wheel rotates about its axle (y-axis) with a speed $-\Omega_y$. When under free rolling conditions and $\alpha=0$ the effective radius is denoted by $R_{eo} = V/|\Omega_{yo}|$, we define the speed of rolling under general conditions:

$$V_r = |\Omega_y| R_{eo} \tag{3}$$

and the longitudinal slip speed:

$$V_{cx} = V_x - V_r . \tag{4}$$

We introduce the two quantities which define the state of slip under straight line rolling, viz., the longitudinal slip s_x and the lateral or side slip s_y:

$$s_x = V_{cx}/V_x = 1 - \Omega_y/\Omega_{yo} \tag{5}$$

$$s_y = V_{cy}/V_x = \tan \alpha \tag{6}$$

In general, also a turn slip due to a rotational speed Ω_z about the vertical z-axis will occur.

The base point B of the tread element (Figs. 1,3) has speed components:

$$V_{Bx} = V_{cx} - \tilde{v}_c \Omega_z \tag{7}$$

$$V_{By} = V_{cy} + (x + \tilde{u}_c)\Omega_z \tag{8}$$

The sliding speed of the contact point (tip of element relative to the road) is given by:

$$V_{sx} = V_{cx} - (\tilde{v}_c + v)\Omega_z + \dot{u} \; , \tag{9}$$

$$V_{sy} = V_{cy} + (x + \tilde{u}_c + u)\Omega_z + \dot{v} \; . \tag{10}$$

For motions with relatively long wavelengths, the terms with Ω_z may be neglected. Henceforth we shall disregard the influence of the rotational speed and use the equations:

$$V_{sx} = V_{cx} + \dot{u} \; ,. \tag{11}$$

$$V_{sy} = V_{cy} + \dot{v} \; . \tag{12}$$

The tread element moves through the contact range with a speed equal to the rolling speed V_r. The contact length is denoted by L = 2a and the time for one run through the contact patch becomes

$$\Delta t = L/V_r \tag{13}$$

Note that the run time tends to infinity when the wheel is locked. This limits the analog simulation to s_x values smaller than unity. As soon as the element has reached the end of the contact length (trailing edge) a new element is assumed to enter at the leading edge. The i-th run starts at the instant t_{i-1} and ends at $t_i = t_{i-1} + \Delta t$.

Coordinate x of the base of the element is determined by:

$$x = \frac{1}{2} L - V_r(t - t_{i-1}) \tag{14}$$

The element has stiffnesses k_x and k_y and damping coefficients c_x and c_y in x and y direction, respectively. At the tip of the element a concentrated mass, m, is considered to be present. The quantities k_x and k_y, c_x and c_y, and m are taken per unit length of circumference. The same holds for the shear force components q_x and q_y and the vertical pressure distribution q_z.

The following equations govern the motion of the element.

$$m \ddot{u} + c_x \dot{u} + k_x u = q_x \tag{15}$$

$$m \ddot{v} + c_y \dot{v} + k_y v = q_y \tag{16}$$

The initial conditions of the deflections and the time rate of change of the deflections of the tread element at $t = t_{i-1}$ are assumed to be equal to zero.

When the resulting shear force opposes the sliding speed, we have:

$$q_x = -q \, V_{sx}/V_s \tag{17}$$

$$q_y = -q \, V_{sy}/V_s \tag{18}$$

with

$$V_s = \sqrt{V_{sx}^2 + V_{sy}^2} \tag{19}$$

Due to the friction law assumed (Fig. 2), we have always:

$$q = \mu \, q_z \tag{20}$$

and the functions

$$\mu = \mu \, (V_s) \tag{21}$$

$$q_z = q_z \, (x) \tag{22}$$

The vertical pressure distribution may be taken as a function of the vertical load $|F_z|$.

The forces and the moment acting on the carcass (i.e., on the wheel) are equal to the integral of the contributions of the internal forces per unit length (acting in spring plus damper of Fig. 1).

$$q'_x = c_x \dot{u} + k_x u \qquad (23)$$

$$q'_y = c_y \dot{v} + k_y v \qquad (24)$$

Figure 4 gives a simplified diagram of the analog circuit which produces the q'_x and q'_y.

The respective integrals determining longitudinal force, lateral force, vertical load and aligning torque read:

$$F_x = \int_{-a}^{a} q'_x \, dx = V_r \int_{t_{i-1}}^{t_i} q'_x \, dt \qquad (25)$$

$$F_y = \int_{-a}^{a} q'_y \, dx = V_r \int_{t_{i-1}}^{t_i} q'_y \, dt \qquad (26)$$

$$-F_z = \int_{-a}^{a} q_z \, dx = V_r \int_{t_{i-1}}^{t_i} q_z \, dt \qquad (27)$$

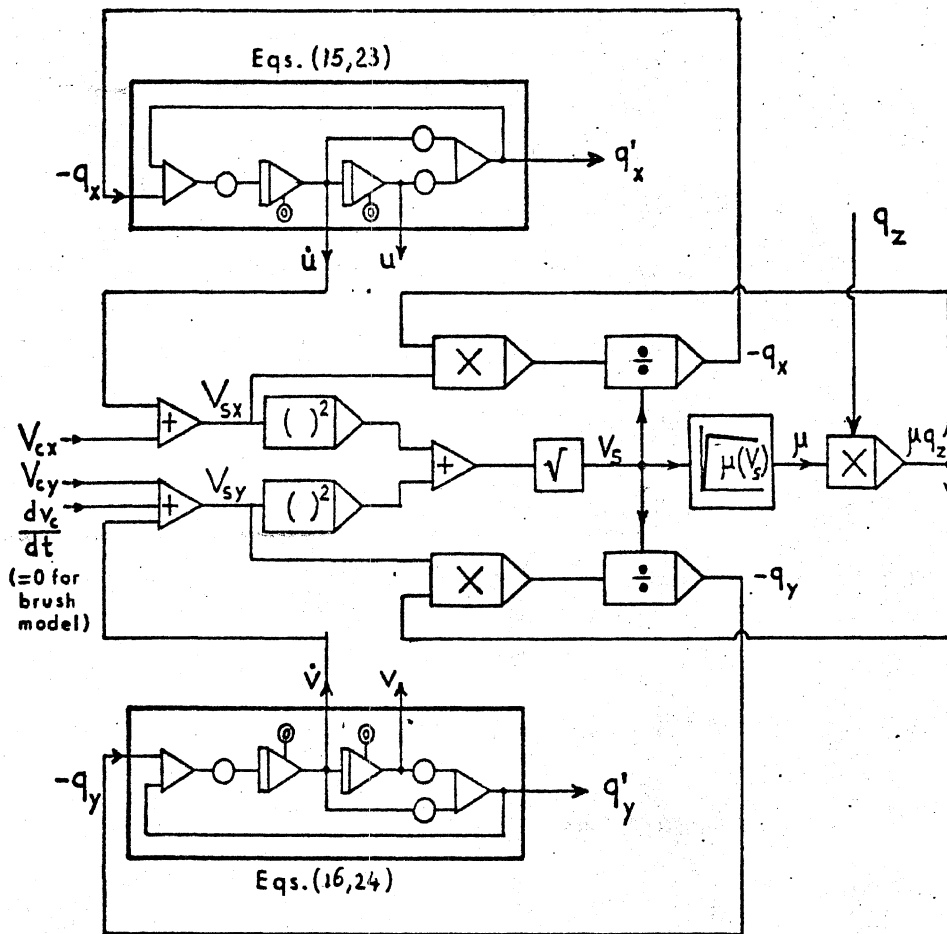$$M_z = V_r \int_{t_{i-1}}^{t_i} \{(x + \tilde{u}_c + u)q'_y - (\tilde{v}_c + v)q'_x\}dt \qquad (28)$$

Figure 4. Simplified diagram of computer circuit for the simulation of tire tread element dynamics.

The effective uniform carcass deflections are defined by
the relations:

$$\tilde{u}_c = \beta_x u_c = \beta_x F_x / K_x \qquad (29)$$

$$\tilde{v}_c = \beta_y v_c = \beta_y F_y / K_y \qquad (30)$$

where K_x and K_y are the carcass stiffnesses and β_x and β_y the
effective fractions which take into account the longitudinal
and lateral rolling deformation of tire with respect to rim and
road (displacement of vertical pressure center).

The moment may be rewritten now as follows:

$$M_z = V_r \int_{t_{i-1}}^{t_i} \{(x + u)q'_y - v q'_x\}dt + \left(\frac{\beta_x}{K_x} - \frac{\beta_y}{K_y}\right)F_x F_y \qquad (31)$$

The values of F_x, F_y and F_z are available at the end of each run.
Since at that instant the product $F_x F_y$ is available, the moment
M_z can also be computed in one run. Figure 5 gives the simplified
diagram for the forces and moment generation. The input quantities
V, α and s_x are either given in the digital program (result from
an input matrix or from the instantaneous conditions of a digital
vehicle motion simulation) or are read from voltages (set by
potentiometer, or resulting from an analog motion simulation). As
soon as comparator 1 gets low (logic 1 at complemented output),
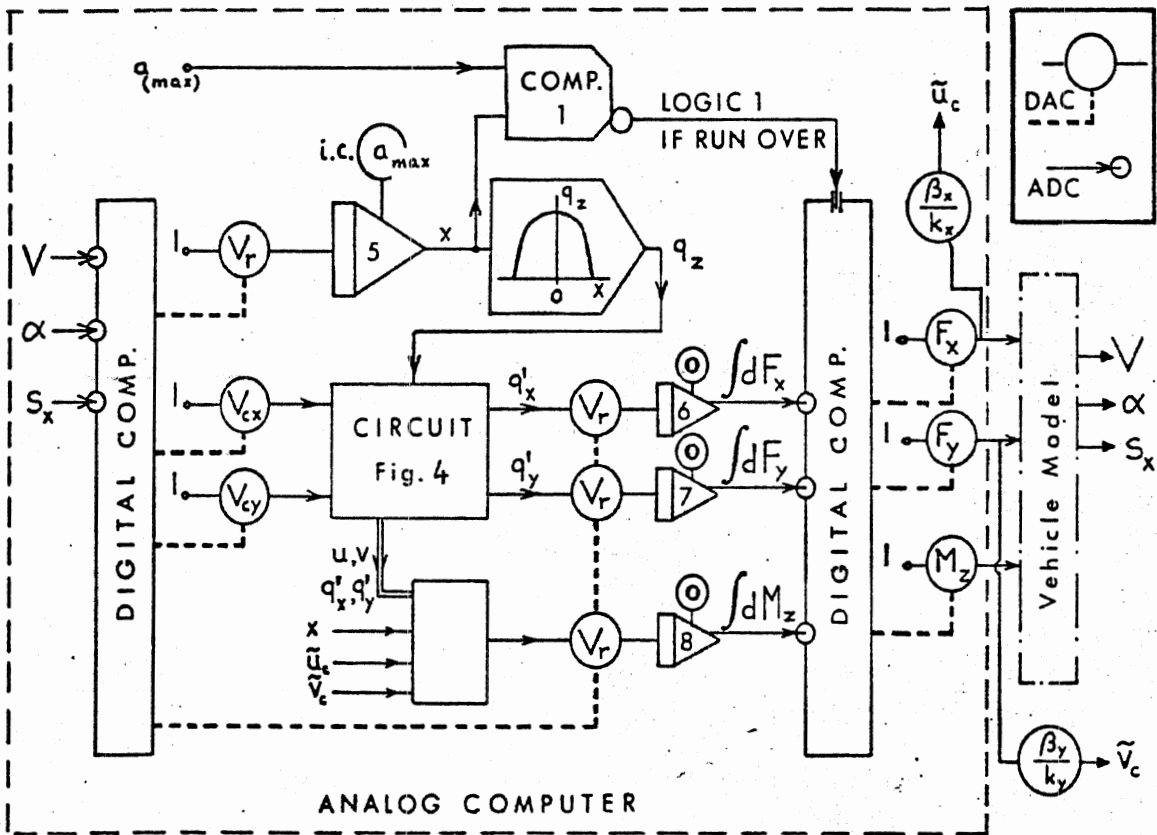the run through the contact patch is terminated and the digital

13

Figure 5. Generation of forces F_x and F_y and moment M_z.

computer puts the analog computer in Hold. The integrated out-
puts are read by the analog to digital converters (ADC's) together
with possible new V, α and s_x values. The values of F_x, F_y and
M_z and the input quantities are stored on tape or printed out
directly and the computed values of V_r, V_{cx} and V_{cy} are set by
the digital to analog converters (DAC's). Subsequently, the
Initial Condition and then the Operate state of the analog
computer are called after which the next run starts.

14

Figure 6 gives the results in graphic form. The complete traction field is shown for a particular tire model and road surface combination. A good qualitative correspondence with known experimental curves appears to arise. The influence of changing the lateral tread element stiffness is shown in the upper right diagram.

The relative simplicity of the circuit and the qualitatively correct results makes the concept interesting for use in connection with automobile motion simulation.
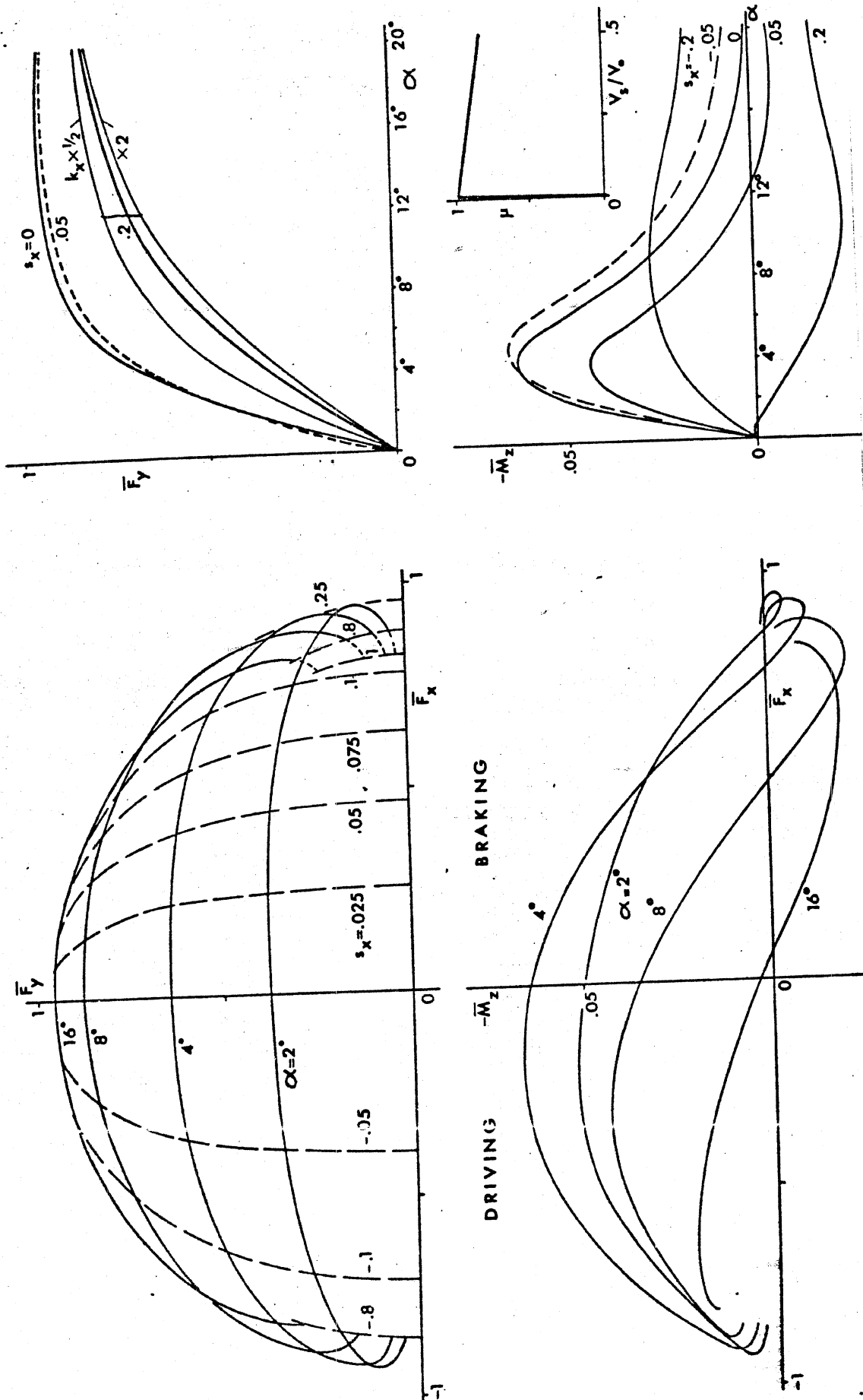
Fig. 6 Traction field for brush type tire model ($\overline{F} = F_x/F_z$, $\overline{F} = F_x/F_z$, $\overline{F} = F_y/F_z$, $\overline{M}_z = M_z/F_z\ell$, ($\overline{F} = F_x/F_{x_0}$), $F_x < 0$); vertical force $F_z = 10^3$ ($V^2 = 10^0$ ft/sec) Parameters: $\ell = 2a$, $q_{z0} = |F_z|/\ell$ (also 10 and 40 q_{z0}/ℓ), $c^0 = c_x = 2$ q_{z0}/V, $m = 0.1$ $q_{z0}\ell/V_o^2$, $k_x = 25$ q_{z0}/ℓ, $k_z = 20$ q_{z0}/ℓ (also 10 and 40 q_{z0}/ℓ), $c^0 = c_x = 2$ q_{z0}/V, $m = 0.1$ $q_{z0}\ell/V_o^2$, $K^y = 11$ q_{z0}, $K = 14$ q_{z0}, $\beta_x = 0.25$, $\beta_v = 0.8$, $q_{zmax} = 1.25$ q_{z0}, $\mu = 1 - 0.353$ V_s/V_o, Influence of y slip angle α and fore and aft slip s_x. Influence of longitudinal element stiffness k_x.

3. MODEL WITH FLEXIBLE CARCASS

Figure 7 depicts the tire model showing a carcass which can not only deform sideways and in longitudinal direction, but which can also show a curved deflection line governed by external forces and by the flexural properties of the tread band and elastic properties of its foundation.
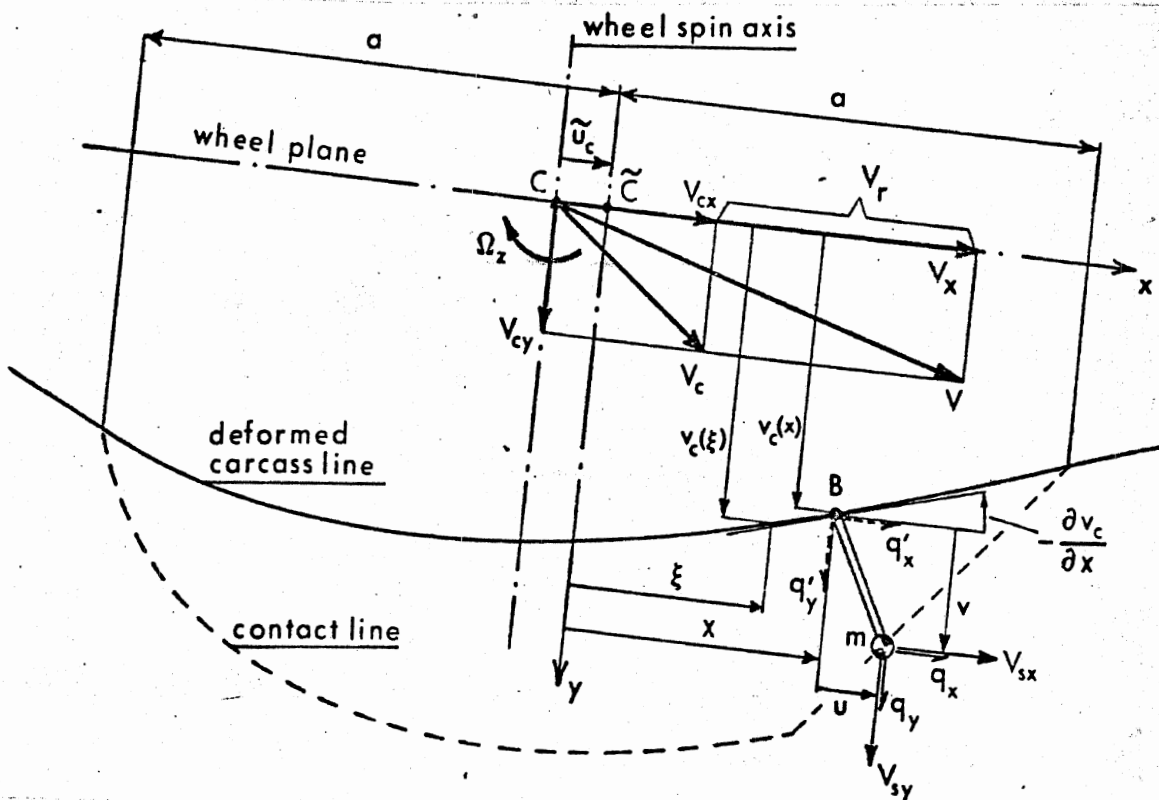

Figure 7. The tread element attached to the deflected flexible carcass

In contrast to the motion of the elements of the rigid carcass model, the base, B, of the element will move along a curvilinear path. The speed of B is influenced by the varying slope of the center line of the carcass. As before, the carcass is assumed to be inextensible in longitudinal direction. It may, however, show a uniform longitudinal deflection $\tilde{u}_c$ under the action of F_x.

The lateral force distribution q'_y causes the carcass to deflect. The influence of the moment distribution, $q'_y u - q'_x v$, upon the deflection is neglected. It is assumed that the elastic properties of the carcass can be considered linear. We may then describe the elastic field of the carcass by means of influence (Green) functions $G(\xi,x)$. This function gives the deformation at coordinate ξ due to a unit force acting at coordinate x. The lateral deformation $d\, v_c(\xi)$ due to a lateral force $q'_y(x)dx$ becomes

$$d\, v_c(\xi) = G(\xi,x)\, q'_y(x)dx \tag{32}$$

The deflection due to the complete force distribution over the contact length is found by the integral:

$$v_c(\xi) = \int_{-a}^{a} G(\xi,x)\, q'_y(x)dx \tag{33}$$

The velocity of the base point, B, of the element with respect to the road surface becomes:

$$V_{Bx} = V_{cx} - v_c(x)\Omega_z + \frac{d\tilde{u}_c}{dt} \tag{34}$$

$$V_{By} = V_{cy} + (x+\tilde{u}_c)\Omega_z + \frac{dv_c}{dt} \tag{35}$$

The lateral speed of B with respect to the wheel plane is given
by the time derivative of v_c. This deformation is both a function
of time, t, and coordinate, x.

$$\frac{dv_c}{dt} = -V_r \frac{\partial v_c}{\partial \xi} + \frac{\partial v_c}{\partial t} \; . \tag{36}$$

In case we deal with a cambered wheel with angle of tilt γ,
the carcass center line is already deflected with respect to the
x-axis (defined as line of intersection of wheel center plane
and road surface) when loaded on a perfectly slippery surface
($\mu=0$). This deflection will be approximated by a parabola (cf.
Fig. 8):

$$d_c = -(C_\gamma + 1/2 \, A_\gamma \, x^2)\gamma \tag{37}$$

The additional deflection v_c exhibited by the carcass when rolling
over a rough surface is brought about by frictional forces q_y. The
expression for the lateral velocity of base point B must now be
extended with the terms $V_r \, \partial d_c/\partial x - \partial d_c/\partial t$ of which the last
term may be neglected for slowly varying camber angles. The last
term of (34) and (36) will, in general, be small too. We retain
the latter, however, because it has a favorable effect on the
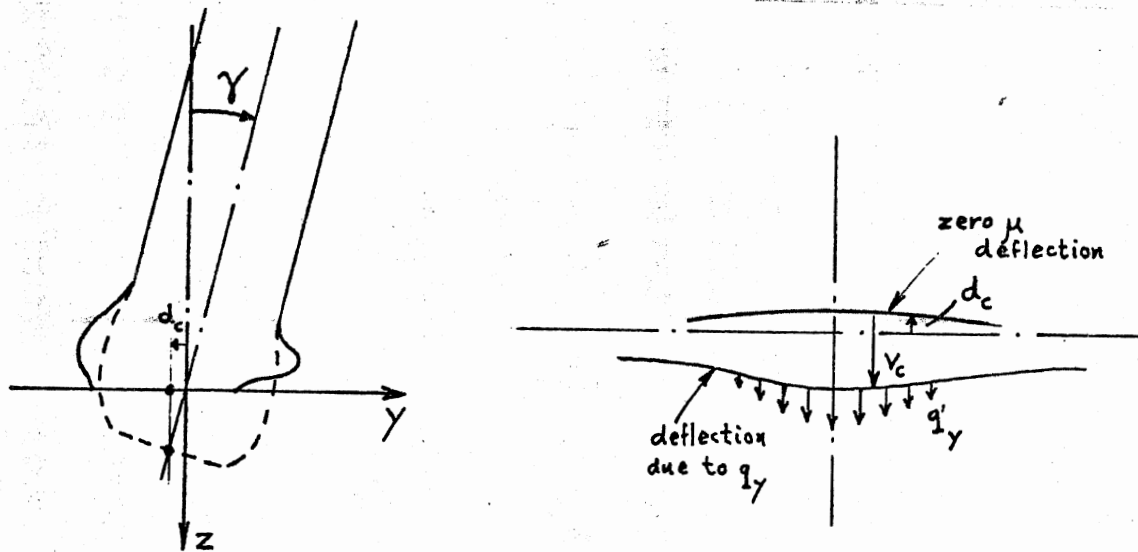stabilization of the analog solution.

19

Figure 8. Deflections due to camber

The sliding speed of the tip of the element with deflections (u,v) reduces to the following form after retaining only the more important terms (relatively slowly varying wheel motions, $\Omega_z \to 0$, $d\tilde{u}_c/dt \to 0$, $\partial d_c/\partial t \to 0$):

$$V_{sx} = V_{Bx} + \frac{du}{dt} \simeq V_{cx} + \frac{du}{dt} \tag{38}$$

$$V_{sy} = V_{By} + \frac{dv}{dt} \simeq V_{cy} - \left(V_r \frac{\partial v_c}{\partial \xi} - \frac{\partial v_c}{\partial t}\right)_{\xi=x} - V_r A_\gamma x\gamma + \frac{dv}{dt} \tag{39}$$

The terms V_{cx}, V_{cy} and $V_r A_\gamma x\gamma$ represent the input quantities to the tire system. The last terms in (38) and (39) are a result

20

of tread element dynamics governed by Eqs. (15) through (22).
The remaining terms of (39), which represent the time rate of
change of carcass deflection at the moving point B, also given
by (36), are governed by the function (33).

The deflections $v_c(\xi)$ can be calculated from (33) once
the q'_y distribution is known. On the other hand, from the
Eqs. (39) and (15) through (24), it is clear that $q'_y(x)$ can
only be calculated for a known carcass deflection $v_c(\xi)$. Evidently,
some kind of iteration process is required for solving the problem.
An obvious procedure would be to leave $v_c(\xi)$ and all input quantities
constant during the time interval needed for the element to
travel through the contact zone. The q'_y distribution can then be
calculated during this run. By simultaneously computing the
integral (33) at a sufficient number of points along the contact
line, the new $v_c(\xi)$ may be found at the end of the run by inter-
polation between the v_c's computed at these points. From the
interpolation formula, the slope $\partial v_c / \partial \xi$ may be obtained as a
function of x. During the next run $v_c(\xi)$ is kept constant and
the function for the slope is used in Eq. (39) for the calculation
of the new $q'_y(x)$. This iteration procedure, however, is bound
to diverge for tire models with tread element lateral stiffness
per unit length much larger than the resulting carcass lateral
stiffness divided by the contact length, as usually is the case
in practice (see discussion in Section 4.2).

In order to avoid this oscillatory divergent result, we may try to more closely approach the way the real tire finds the solution. The carcass deflection will not be held constant during a passage but is allowed to change as a result of the difference of $q'_y(x)$ with respect to the $q'_y(x)$ encountered in the previous run. The following equations apply for the i-th run:

$$\Delta q'_y(x) = q'_y(x) - q'_{y_{i-1}}(x) \tag{40}$$

$$v_c(\xi,t) = V_r \int_{t_{i-1}}^{t} G(\xi,x)\, \Delta q'_y(x)\,dt + v_{c_{i-1}}(\xi) \tag{41}$$

with

$$x = \frac{1}{2} L - V_r(t-t_{i-1}) \tag{42}$$

At each instant, the $v_c(\xi)$ is available and is a result of the new q'_y distribution generated over the x range already covered by the moving element plus the old q'_y distribution of run i-1 over the range not yet covered by the element. The instantaneous value of the slope $\partial v_c/\partial \xi$ at $\xi=x$ may be calculated and fed into Eq. (39).

Since the carcass deflection changes in time due to the difference $\Delta q'_y(x)$, a finite value of $\partial v_c/\partial t$ at $\xi=x$ will be found. When the element is moved over a distance $(-dx)$, the increment in carcass deformation at $\xi=x$ due to $\Delta q'_y$ reads:

$$dv_c = G(x,x) \, \Delta q'_y (-dx) \tag{43}$$

so that, in view of (42), the partial derivative with respect to time (ξ fixed) becomes:

$$\left(\frac{\partial v_c}{\partial t}\right)_{\xi=x} = V_r \, G(x,x) \, \Delta q'_y \tag{44}$$

This term, although small, may be retained in the computation as it turns out to be of great value for the stabilization of the iteration.

The generation of the difference $\Delta q'_y$ by the hybrid computer, using Eq. (40), requires a memory device. We have chosen to use the digital computer for this purpose. The passage time is divided up in N (say 20) equal steps. At the end of each step (k) the q'_y value is transmitted to the digital computer and stored in the first location of an array. Before this is done, all the N elements of the array containing the q'_y values obtained at the ends of the previous steps are shifted one location downwards so that the first location becomes empty and is ready to receive the new q'_y value. Before this shift is executed, the last two values of the array are read and transmitted to the analog computer. These two values are the q'_y values of the previous run at the beginning and end of the next step (k+1). By linear interpolation between these two values, the old $q'_{y_{i-1}}$ value

may then be found as a function of x for x lying in between
the step limits. We obtain during step (k) with limits x_{k-1}
and x_k:

$$q'_{y_{i-1}}(x) = q'_{y_{i-1}}(x_{k-1}) + \frac{x_{k-1} - x}{x_{k-1} - x_k} \{q'_{y_{i-1}}(x_k) - q'_{y_{i-1}}(x_{k-1})\}$$

(45)

The generation of the function for the carcass deflection $v_c(\xi)$
at a given instant of time may be accomplished approximately
by interpolating between the values found by conducting the
integration (41) at a number of discrete points in the contact
zone, for instance: the leading edge (x=a), the center (x=0),
and the trailing edge (x=-a). We have respectively:

$$v_{c1} = V_r \int_{t_{i-1}}^{t} G_1(x) \, \Delta q'_y(x) \, dt + v_{c1_{i-1}}$$

$$v_{c0} = V_r \int_{t_{i-1}}^{t} G_0(x) \, \Delta q'_y(x) \, dt + v_{c0_{i-1}}$$

$$v_{c2} = V_r \int_{t_{i-1}}^{t} G_2(x) \, \Delta q'_y(x) \, dt + v_{c2_{i-1}}$$

(46)

where

$$v_{c1} = v_c(a), \quad v_{c0} = v_c(0), \quad v_{c2} = v_c(-a)$$

$$G_1(x) = G(a,x), \quad G_0(x) = G(0,x), \quad G_2(x) = G(-a,x)$$

(47)

24

Interpolation yields:

$$v_c(\xi) = a_0 + a_1\xi + a_2\xi^2 \tag{48}$$

The slope at $\xi = x$ reads:

$$\left(\frac{\partial v_c}{\partial \xi}\right)_{\xi=x} = a_1 + 2a_2 x \tag{49}$$

The coefficients are found by satisfying the deflection (46). A more stable solution for large numbers of runs through the contact patch may be obtained by taking the slope (49) at $\xi = a$ equal to $-v_{c1}/\sigma$. The length σ is determined from the almost exponential shape of the outer portion of the Green function. Calculation of only $\ddot{v}_{c1}$ and v_{c2} may be sufficient in this case (cf. discussion in Sec. 4.3). With (44) and (49), the "remaining" terms of the formula for the sliding speed in lateral direction (39) have been determined.

The forces F_x, F_y and F_z and the moment M_z may be obtained by conducting the integrations (25) through (28) and updating at the end of each run. Since we have now the increment $\Delta q'_y$ at our disposal, we may as well generate a more continuous variation of F_y by employing the integral:

$$F_y = V_r \int_{t_{i-1}}^{t} \Delta q'_y(x)\,dt + F_{y_{i-1}} \tag{50}$$

where $F_{y_{i-1}}$ represents the value of F_y at the end of the previous passage $(i-1)$.

Figure 9 gives a diagrammatic picture of the hybrid computer circuit for the generation of carcass deflection and side force. Appendix IV presents the complete diagrams and digital program in its most recent form after the modifications discussed in Section 4.4 have been introduced. The influence functions G_1, G_0, and G_2 employed are assumed identical except that they are shifted sideways over a distance, $a = \frac{1}{2} L$, with respect to each other. In reality, for a loaded tire, the function G_0 measured at the center may differ from the other two which are measured at the ends of the contact patch. A method for measuring influence functions of loaded tires has been developed by Savkoor [6]. Note that for our purpose the tread rubber should be buffed off first. The Green functions used are in Appendix IV (Fig. 25). They are taken from deflection curves shown by Frank [2] for a radially unloaded tire. The tire was axially loaded by a concentrated force. In general, the Green functions will change when a radial load is applied as well.
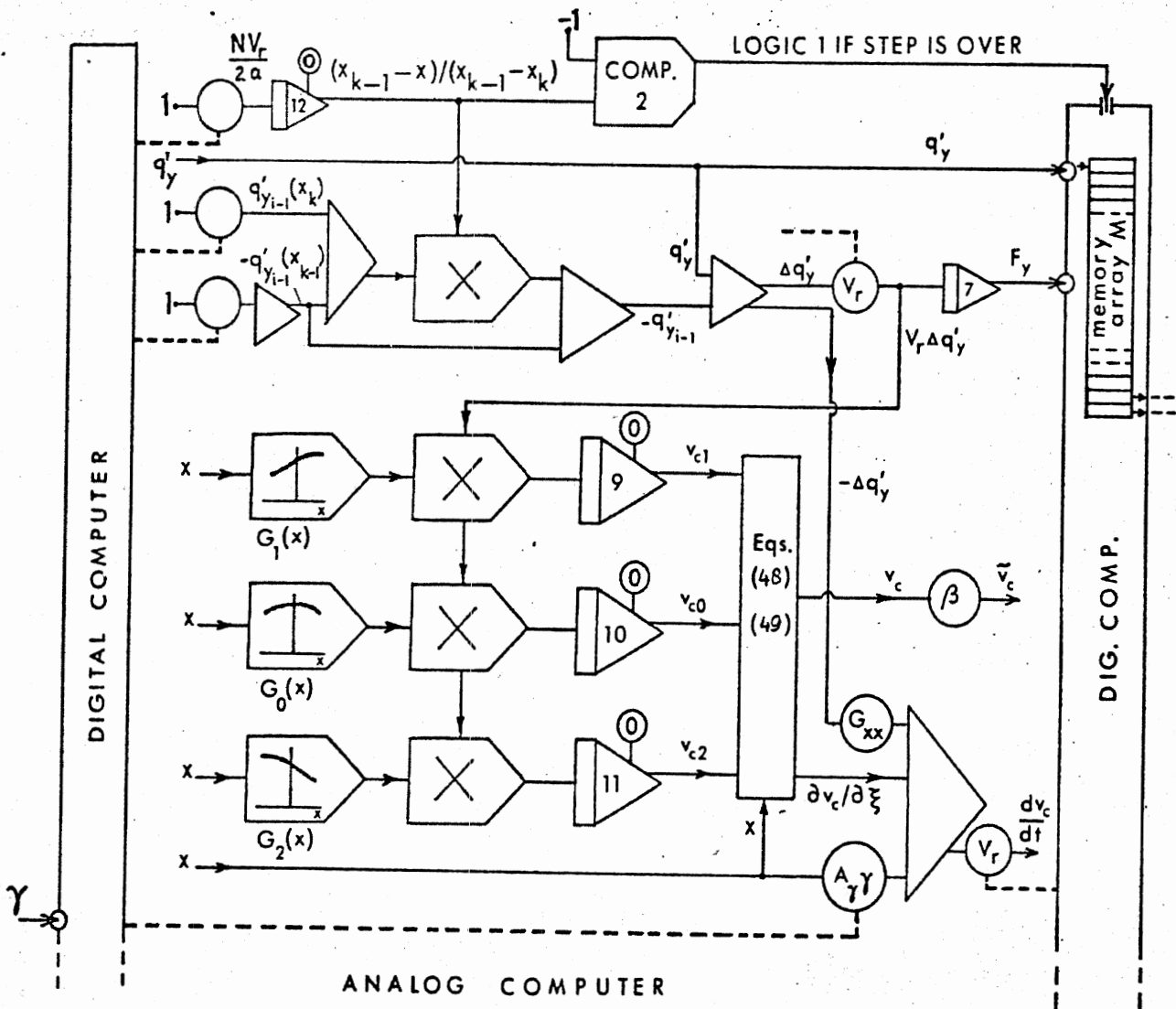
Figure 9. Simplified block diagram of circuit for generation of
carcass deflection and side force. The diagram must be
used in connection with the diagram shown in Fig. 5.
The moment M_z will be computed in a slightly different
way, however. At the end of each step (signalized by
comparator 2) integrator 12 is set in Initial Condition
and the remaining integrators in Hold. The last two
elements are read and transmitted to the DAC's for the
generation of the q'_y of the previous run. Then the
array is shifted one place, the now empty first array
element is then filled with the new q'_y obtained from
the ADC. At the end of these operations, the system is
set in Operate and the subsequent step begins. At the
end of the run indicated by comparator 1 (Fig. 5) (make
a, slightly less than $|X_N| = \frac{1}{2}L$) the procedure as des-
cribed in the caption of Fig. 5 is followed in addition
to operations done at the end of each step with the
exception that after the shift, the last element of the
array is made equal to zero representing the q'_y value
at the beginning of the contact patch. The integrators
7, 9, 10 and 11 remain in the Hold state before calling
Operate.

The flow diagram of the digital program shown in
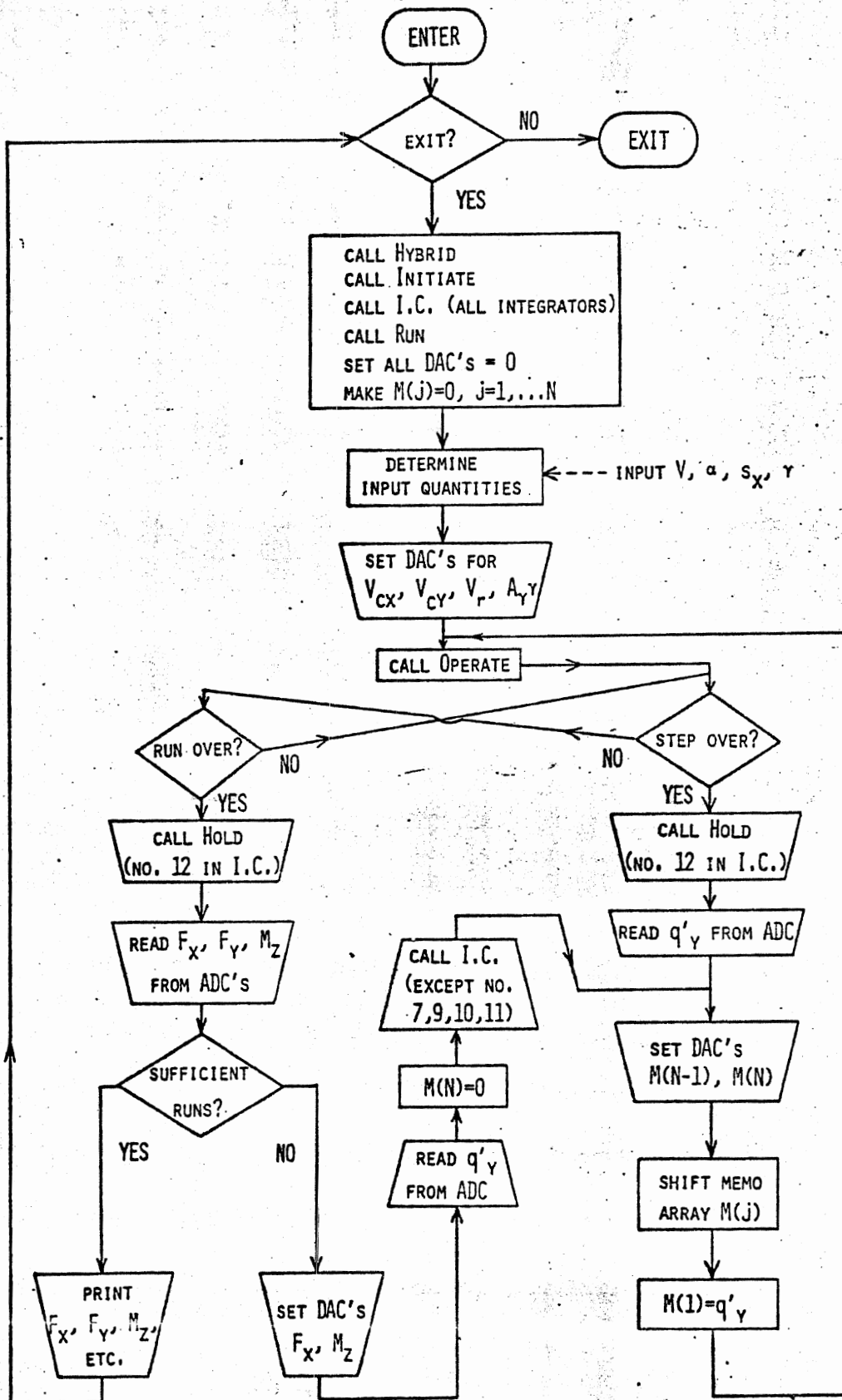Fig. 10 clarifies the situation.

27

Figure 10. Flow diagram of digital computer program. The inputs may be entered through ADC's, key-board or may be listed in the digital program.

Two collections of computer results have been shown in Figures 11 and 12. They present the complete steady-state traction fields for two different μ functions. Figure 11 shows the five related diagrams $(F_y - \alpha)$, $(F_y - F_x)$, $(F_x - s_x)$, $(M_z - F_x)$, $(M_z - \alpha)$. In the $(F_y - \alpha)$ diagram the curve produced by a combination of camber angle γ and slip angle α has been shown. Also, the influence of lowering the carcass foundation stiffness (Green functions larger) and at $s_x = 0.2$ the influence of a change in longitudinal stiffness K_x have been indicated. The $(F_y - F_x)$ diagram shows curves for constant values of α and s_x. At low slip angles the α-curves tend to rise at increasing braking force until a maximum is reached. The carcass flexibility appears to enhance this phenomenon (compare Fig. 6). The sign change of M_z which occurs beyond a certain braking force range is due to the displacement of the line of action of F_x which could already be accomplished with the simpler model (Fig. 6). Experiments substantiate this phenomenon. The realistic appearance of the responses to step functions of the slip angle shown in Figure 11 suggests that the model is capable of simulating a tire's transient behavior. Figure 12 presents curves which may be encountered on wet slippery roads (dashed μ-curve of Fig. 24). Again, experiments substantiate the qualitative aspects of the theoretical results. The increase in F_y and M_z at small α-values as a result of an increase in V is caused by the presence of damping in the tread elements. The decaying μ-function is responsible for the sign change of M_z at larger values of α (also when $s_x = 0$). Appendix IV presents parameter values and functions used in these calculations.
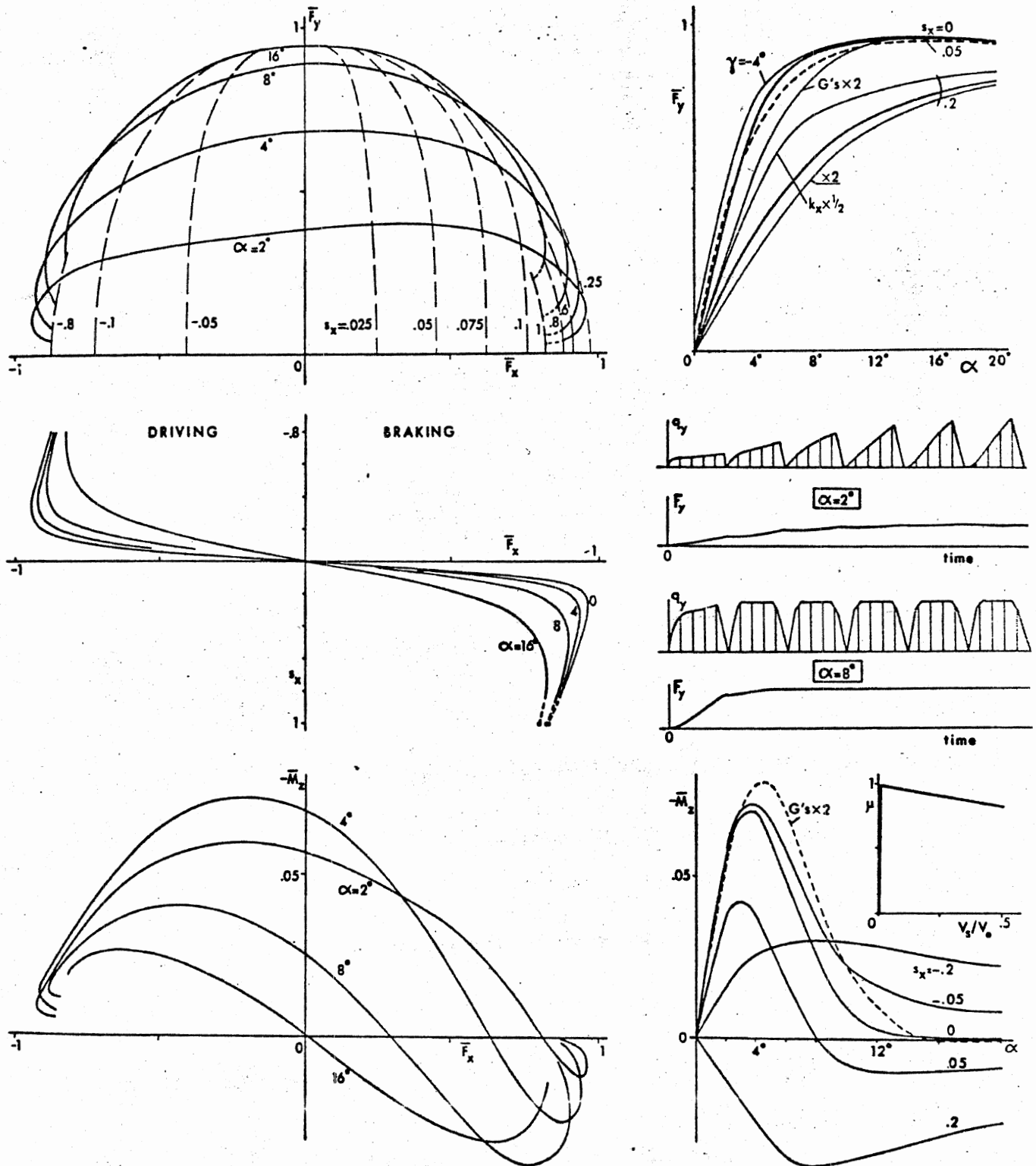
Fig.11 Traction field for flexible carcass tire model (computed with G_1 and G_2 for $\sigma=4a$). Parameters as in Fig. 3 except: $k_y=40 \, q_{zo}/\ell$, $K_y=0$ but $G(a,a)=0.128/q_{zo}$, $G(a,-a)=0.085/q_{zo}$; $A_y=0.7/\ell$. Influence of variables α, s_x and camber angle γ. Influence of stiffness parameters k_x and $G(\xi,\hat{x})$. Built up of lateral force F_y and lateral force distribution q_y as a response to step input of slip angle α.
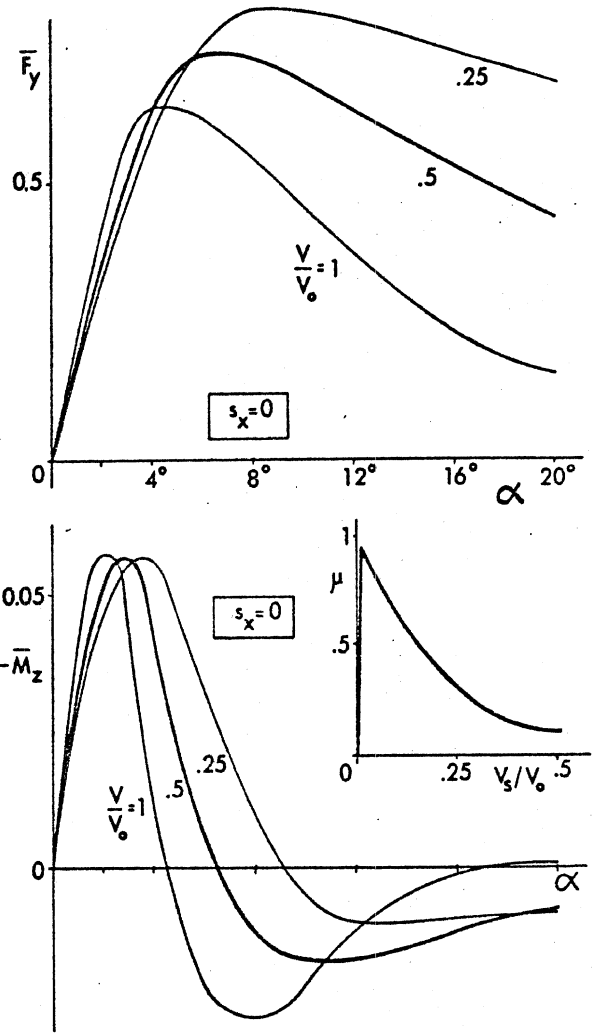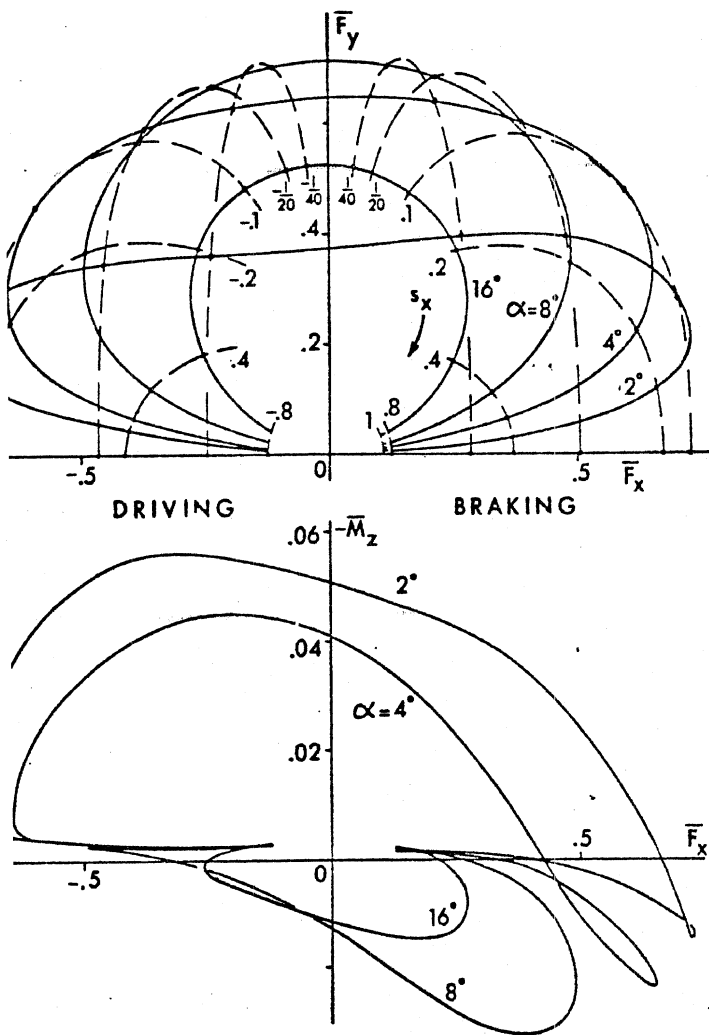
Fig. 12 Traction field on surface with sharply decaying μ-curve. Parameters as in Fig. 7 except $c_x = c_y = 6 \; q_{zo}/V_o$. Influence of variables $α$, s_x and V.

4. INSTABILITIES

In this section we shall deal with instabilities which turned up during the calculations and which are partly due to model properties and partly due to computational methods which have been adopted.

4.1 SLIP-STICK

The elastic tread element which slides over the ground is capable of showing an unstable oscillatory motion when the coefficient of friction exhibits a decaying function with sliding speed (Fig. 2), i.e., when the derivative

$$\frac{d\mu}{dV_s} < 0, \tag{51}$$

and, moreover, when it does not have sufficient internal damping to suppress this instability.

The equation for the element shown in Figure 1 reads when only lateral motions are considered ($V_{cx} = V_{Bx} = 0$).

$$m\, \ddot{v} + k_y \dot{v} + c_y v = q_y$$

with

$$q_y = -\mu\, q_z\, \text{sgn}\, V_s$$

The sliding speed equals

$$V_s = V_{By} + \dot{v}$$

Assume the μ-characteristic shows a slope

$$\frac{d\mu}{dV_s} = -b$$

at the steady-state speed $V_s = V_{By}$. Around this equilibrium situation we have consequently:

$$\mu = \mu_o - b(V_s - V_{By}) = \mu_o - b\,\dot{v}$$

The equation of motion reads now (assume $V_s > 0$):

$$m\ddot{v} + (k_y - bq_z)\dot{v} + c_y v = \mu_o q_z \qquad (52)$$

Hence instability will arise for

$$k_y < bq_z \qquad (53)$$

The q'_y distribution observed for zero or small damping coefficient c_y indeed showed oscillations which were particularly violent when the dashed μ-function of Figure 24 was used. Figure 13 shows an example. In the actual calculations the damping has been made sufficiently large in order to suppress the oscillations.
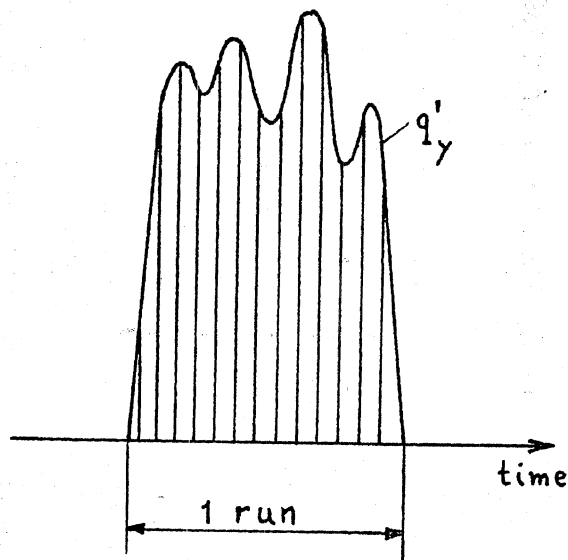
33

Figure 13. Slip-stick observed at low damping c_y

4.2 INSTABILITY OF ITERATION PROCEDURE

Computations carried out with the simple brush-type model have indicated that no computational instabilities whatever occur. This seems logical because the force generation at a particular run does not depend on the results of the previous run.

This is quite different with the more complex model which exhibits carcass flexibility. Three kinds of instability may arise. The first one has been avoided from the outset. This is the oscillatory instability which will occur when the "direct" iteration procedure is chosen which has been outlined before. The deflection of the carcass is obtained directly from the

force distribution, q'_y, which results from the previous run where the carcass deflection has been kept constant. That instability is expected to occur for tire models exhibiting a lateral stiffness of the tread element per unit length which is considerably greater than the lateral carcass stiffness divided by the contact length (which is usually the case with real tires) can be explained by considering the simple two-spring system shown in Figure 14a. During the first run the carcass deflection will be kept equal to zero. The deflections of the tread elements are governed by the slip angle considered. The side force distribution resulting in F_{y1} produce the relatively large carcass deflection used in the second run. With the same slip angle the tread element deflection will now most probably be directed in the opposite sense. Consequently, the carcass deflection for the third run will flip over to the other side. The subsequent carcass deflection of the fourth run will become larger than the deflection of the second run. Obviously, an oscillatory instability arises.
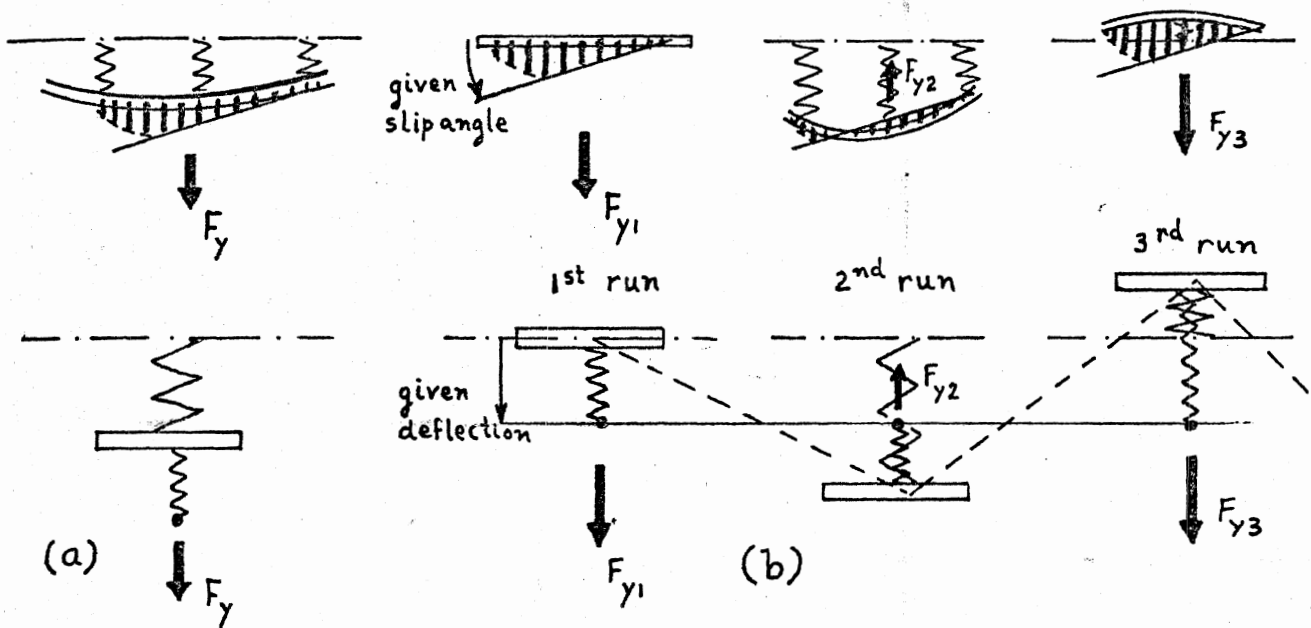
Figure 14. Explaining oscillatory instability occurring
with "direct" iteration procedure

This instability is avoided by not integrating q'_y times
the Green function but the difference of q'_y with respect to
the one encountered at the previous run, $\Delta q'_y$, times the Green
function considered, and then adding the resulting increment
in deflection to the deflection found at the end of the previous
run (the latter is accomplished by keeping the integrators 7,
9, 10 and 11 in Hold when going from one run to the next run,
Fig. 9). In this way the carcass deflection is built up gradually,
much like the real tire does. Already during the first run the
carcass deflection starts to develop (see typical variation of
quantities shown in Fig. 15).

4.3 MODEL INSTABILITIES

In the original configuration, the carcass deflection is calculated by means of a parabolic interpolation between carcass deflections at the leading edge, in the middle, and at the trailing edge. As has been shown in Figure 15, an instability of the shape of the contact line shows up after about 60 runs. The q'_y tends to decrease at the leading portion of the contact length and finally changes sign and grows in the other direction. This turns out to be due to the fact that a smaller v_{c1} (leading edge) leads to a steeper slope of the carcass deflection in the leading contact range. With the slip angle remaining the same, the tread element deflections at the leading range will now become smaller. The resulting smaller q'_y in this range causes a further reduction of the deflection v_{c1} and an increase in slope. Eventually, v_{c1} may change sign.

This phenomenon becomes more severe at smaller slip angles and lower stiffness of the carcass. In order to suppress this kind of instability, we tried to relate the slope at the leading edge to the deflection v_{c1}. From the Green function (= deflection due to concentrated lateral unit force) we found that the deflection varies approximately exponentially. This indicates that the relation

$$\left(\frac{\partial v_c}{\partial x}\right)_{x=a} = -\frac{1}{\sigma} v_{c1} \tag{54}$$

between slope and deflection may be used. The length σ can be determined from the Green function shown in Figure 25. We found σ = 2L = 4a.

This additional condition calls for a cubic instead of a parabolic interpolation. As has been shown in Figure 15, the same kind of instability still shows up but now more towards the middle of the contact length. The deflection v_{c1} does not change in sign but still decreases bringing about a larger slope near the contact center which lowers the q'_y in that range and thereby pushes back the v_{c1} (and to a much lesser extent the v_{c0} and v_{c2}).

Finally, we tried a simpler interpolation by using only the deflections at the leading edges and, furthermore, the tangent relation (54) at the leading edge. The model turns out to be now essentially stable. The parabolic interpolation with tangent relation has been used for the calculation of the graphs 11 and 12.

4.4 DRIFT

Some drift, however, still remains. This slowly developing deviation of deflections and side force could not be explained from model properties. It is believed to be caused by small error voltages which continuously built up. Insufficient feedback in the system is responsible for this weak instability.

The simple rigid carcass model did not suffer from this phenomenon. There, the q'_y is integrated directly, whereas the iteration procedure adopted for the flexible carcass model integrates $\Delta q'_y$. A slight systematic error in the memory process which produces $q'_{y_{i-1}}$, the q'_y distribution of the previous run, gives rise to a non-zero $\Delta q'_y$ also when the steady-state has been attained. This obviously causes a drift of side force and deflections. In order to avoid this drift, an artificial feedback is constructed by integrating q'_y during individual runs distributed over the total computing time. This is accomplished by introducing switches in the analog circuit which in the normal situation make connections so that $\Delta q'_y$ is integrated and, after a command from the digital computer at the beginning of a run, change the circuit in order to integrate q'_y. At the same time, the integrators for F_y and the v_c's are set in Initial Condition and the values for F_y and the v_c's computed at the end of the previous run are stored in DAC's. Additional switches connect the wires which came from the original F_y and v_c outputs to these DAC outputs. At the end of these direct integration runs, the original situation will be restored. In the schemes of Figures 21 and 22, the switches and the accompanying logic are shown.

Figures 17 and 18 present results for the configuration with switches. After each fifth run, the switches change connections and the direct integrations are conducted. The

computations are now completely stable. The discontinuities in the F_y trace point to a slightly incorrect return of the q'_y distribution of the previous run. An improvement of the memory process will certainly improve the results and the switch configuration may even prove to be unnecessary. A continuous memory device like a magnetic tape recorder seems to be most promising.

The instabilities described in Section 4.3 seem to be due to the fact that only a limited number of deflections along the contact length has been computed. The required tangent relation at the leading edge (which is certainly not an elegant solution) would not have been necessary if we had at our disposal a greater number of calculated deflections near the front edge. The real tire which "calculates" the carcass deflection continuously along the contact line manages to get a stable solution.
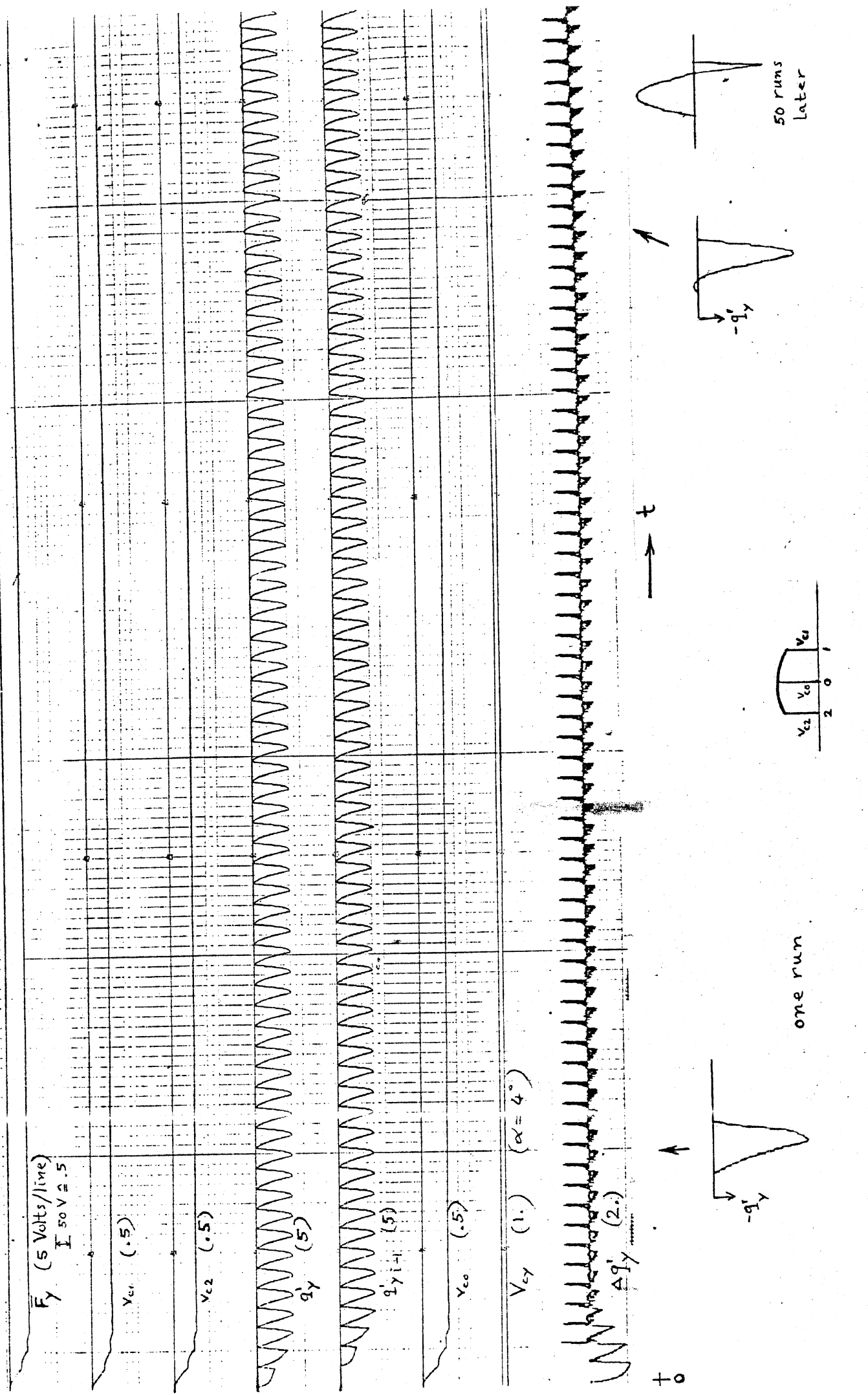
Fig. 15. Parabolic interpolation (original situation)

41
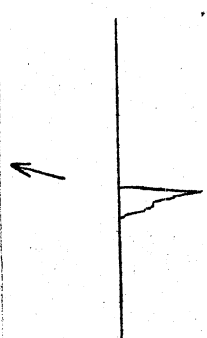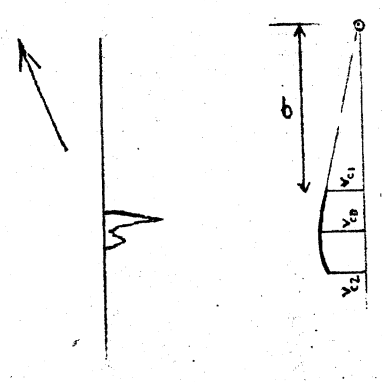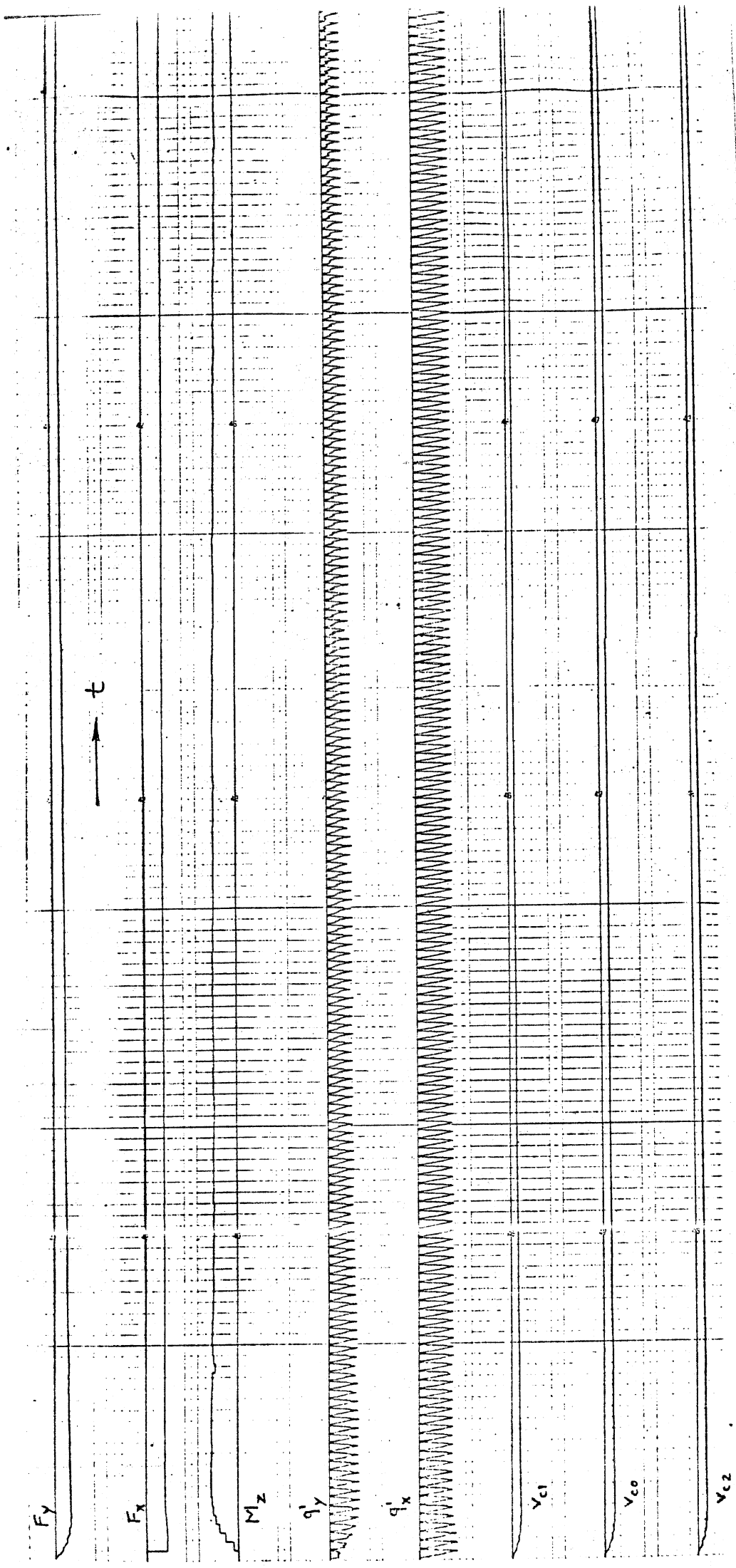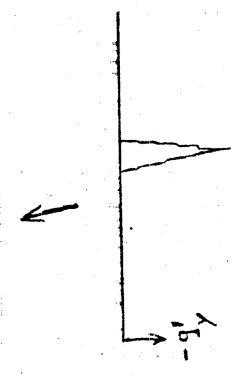
Fig. 16. Cubic interpolation with tangent relation at leading edge

one run

Fig. 17. Latest configuration with switches

Parabolic interpolation with tangent
relation at leading edge
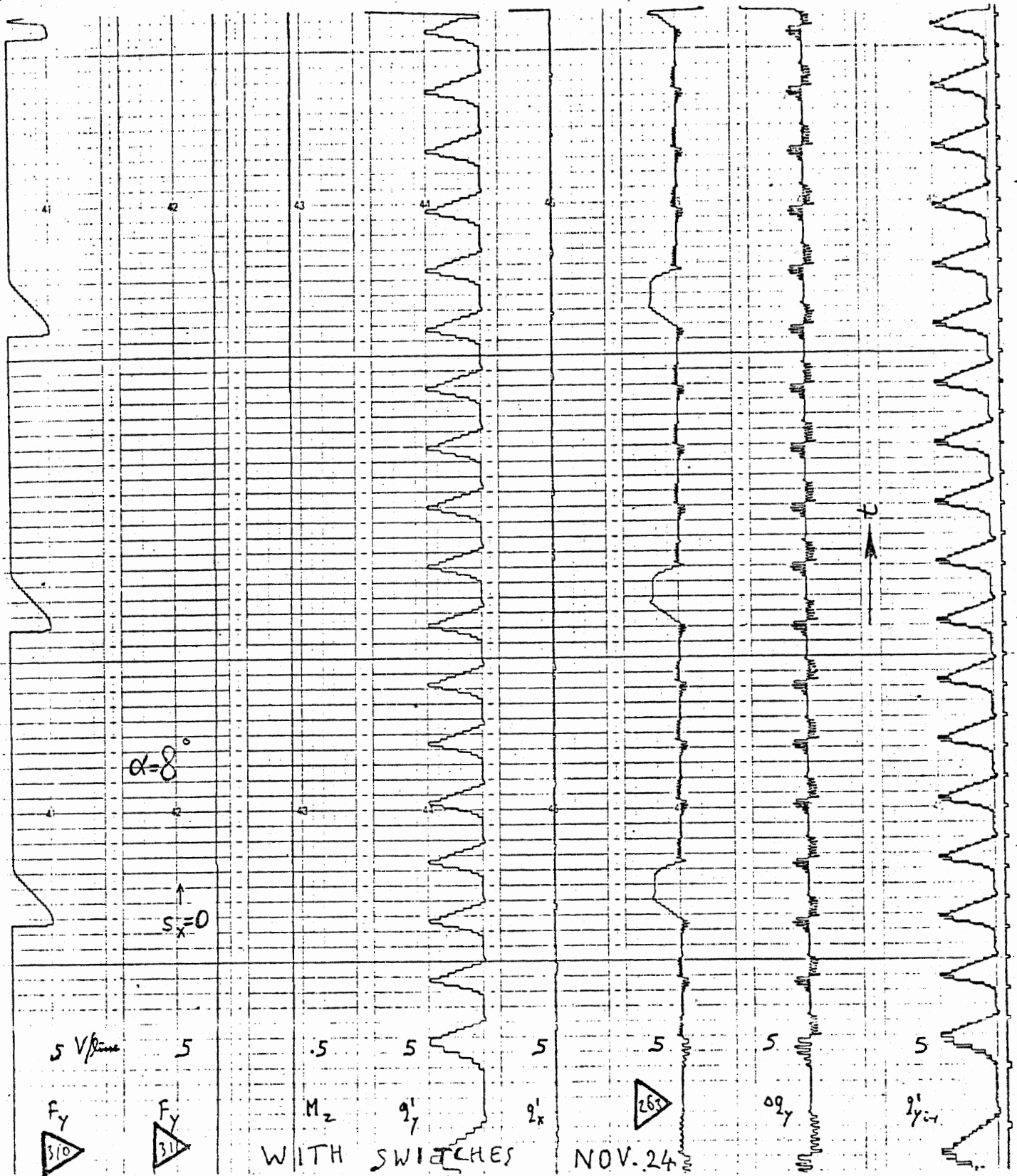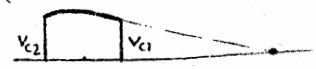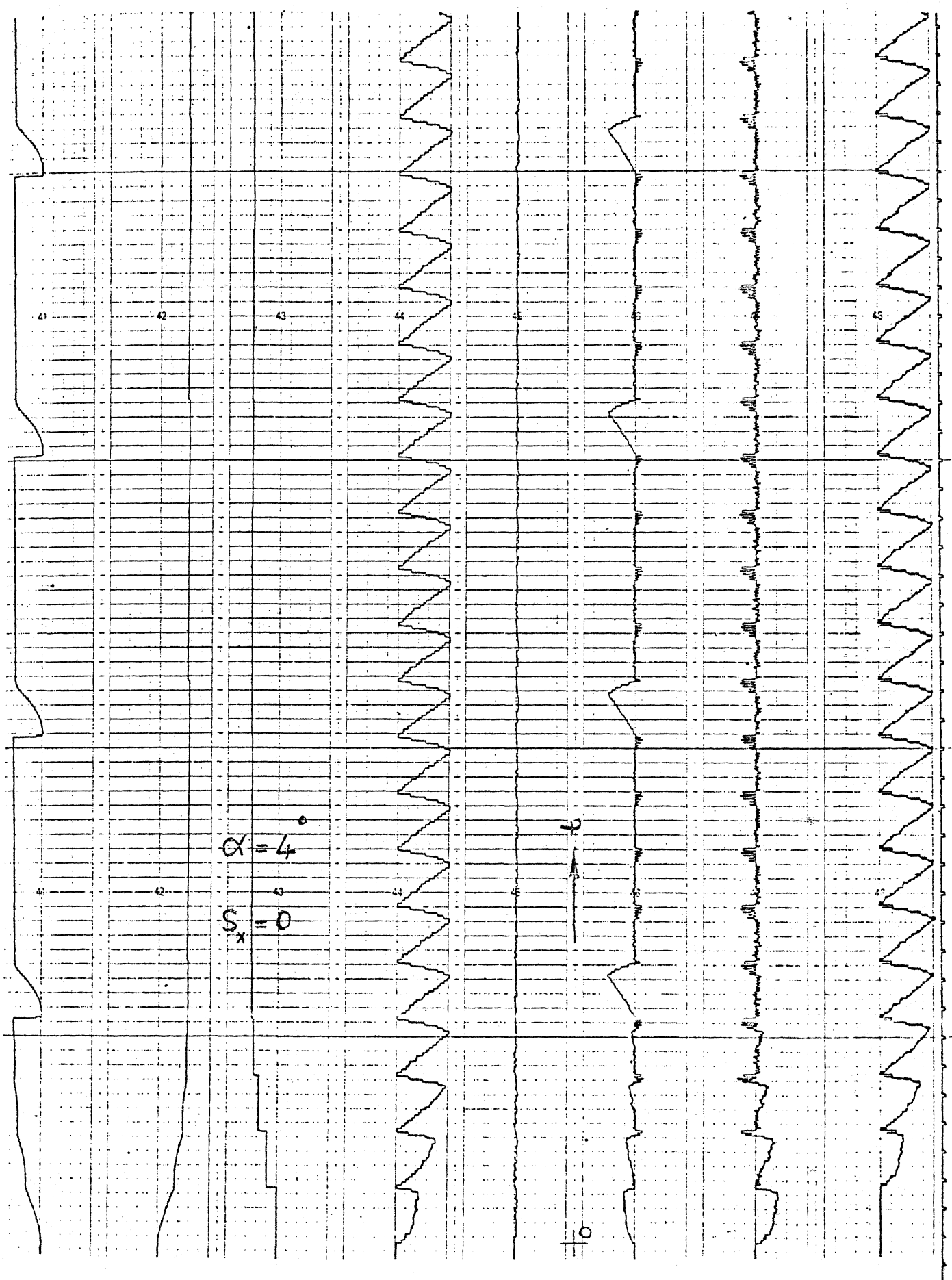
Fig.18   Same as Fig.17, only for $\alpha = 4°$.

5. REFERENCES

1. PACEJKA, H.B., Hybrid Simulation of Shear Force
    Development of a Tire Experiencing Longitudinal
    and Lateral Slip. FISITA Congress, London, 1972.

2. FRANK, F., Grundlagen zur Berechnung der Seitenfuhrungs-
    kennlinien von Reifen. Kautschuk u. Gummi 18
    (1965) 8, p. 515.

3. WILLUMEIT, H.P., Theoretische Untersuchungen an einem
    Modell des Luftreifens.... Dissertation, T.U. Berlin,
    1969.

4. DUGOFF, H., FANCHER, P.S., and SEGEL, L., An Analysis of
    Tire Traction Properties..... FISITA/SAE Congress,
    1970, Paper 700377.

5. PACEJKA, H.B., Dynamic Frequency Response of Pneumatic
    Tires to Lateral Motion Inputs. 2nd Conference on
    Motor Vehicles and Motor Engineering, Sopron
    (Hungary), 1971.

6. SAVKOOR, A.R., The Lateral Flexibility of Pneumatic Tires
    and Its Application to the Lateral Rolling Contact
    Problem. FISITA/SAE Congress 1970, Paper 700378.

APPENDIX I

LIST OF TERMINOLOGY

a	half contact length
A_γ	camber deflection coefficient
B	base-point of tread element
$c_{x,y}$	damping coefficient of tread elements in x,y direction
C	contact center
F_x	longitudinal force acting from road to tire
F_y	lateral force acting from road to tire
F_z	vertical force (= -wheel load)
G	Green function (influence function)
i	number of current run
k	number of current step
$k_{x,y}$	longitudinal, lateral stiffness of tread element
$K_{x,y}$	longitudinal, lateral carcass stiffness
L	contact length
m	effective mass of tread
M_z	aligning torque
N	number of steps in one run

q	shear force from ground to tire (per unit contact length)
$q_{x,y}$	x and y component of q
$q'_{x,y}$	x and y component of force at base-point B
$q'_{y_{i-1}}$	q'_y in previous run
q_z	vertical pressure distribution (≥ 0)
$\Delta q'_y$	difference of q'_y with respect to previous run
R_{eo}	effective rolling radius at free rolling and $\alpha=0$
$s_{x,y}$	longitudinal slip (= $V_{cx}/V \cos \alpha$), lateral slip (= $\tan \alpha$)
t	time
Δt	time needed for element to travel through contact length
u	longitudinal deformation of tread element
$\tilde{u}_c$	longitudinal uniform deformation of carcass
v	lateral deformation of tread element
v_c	lateral deformation of carcass
$\tilde{v}_c$	lateral uniform deformation of carcass
V	speed of contact center (or of wheel center)
V_B	speed of base-point
V_c	slip speed ($\vec{V}_c = \vec{V} - \vec{V}_r$)
$V_{cx,y}$	x and y components of V_c

47

V_o reference speed (100 ft/sec)

V_r speed of rolling = (effective rolling radius at $F_x=0$) × (speed of revolution)

V_s sliding speed of tip of tread element

$V_{sx,y}$ sliding speed in x,y direction

$V_{x,y}$ longitudinal, lateral component of wheel center speed

x longitudinal coordinate (direction)

x_k x at end of k-th step

y lateral coordinate (direction)

α slip angle

$\beta_{x,y}$ reduction factors for effective longitudinal and lateral carcass deflections

γ camber (inclination) angle

μ coefficient of friction

σ relaxation length of free carcass lateral deflection

Ω_y rotational speed of wheel about wheel axle (< 0)

Ω_z rotational speed about vertical axis

ξ longitudinal coordinate

APPENDIX II

NON-DIMENSIONAL QUANTITIES

The actual calculations have been conducted with the aid of non-dimensional equations. We introduce the average vertical load per unit contact length

$$q_{zo} = \frac{|F_z|}{L}$$

where $|F_z|$ is the vertical tire load and L the contact length. Furthermore, we introduce a reference speed

$$V_o = 100 \text{ ft/sec}$$

With the aid of these quantities, we define the following non-dimensional quantities:

vertical load/unit length	$\bar{q}_z = q_z/q_{zo}$
horizontal load/unit length	$\bar{q}_H = q_H/q_{zo}$
Green function	$\bar{G} = G \cdot q_{zo}$
sliding speed, etc.	$\bar{V}_s = V_s/V_o$
time	$\bar{t} = V_o t/L$
machine time	$T = \alpha_T \bar{t}$

derivative $(\dot{\ }) = d(\ )/dT$

longitudinal deflection $\bar{u} = u/L$

lateral deflection $\bar{v} = v/L$
    etc.

longitudinal coordinate $\bar{x} = x/L$

lateral total force $\bar{F}_y = F_y/|F_z|$

longitudinal total force $\bar{F}_x = F_x/|F_z|$

aligning moment $\bar{M}_z = M_z/(L \cdot |F_z|)$

mass per unit length $\bar{m} = mV_o^2/(q_{zo} \cdot L)$

damping per unit length $\bar{c}_{x,y} = c_{x,y}V_o/q_{zo}$

stiffness per unit length $\bar{k}_{x,y} = k_{x,y}L/q_{zo}$

carcass stiffnesses $\bar{K}_{x,y} = K_{x,y}L/|F_z|$

friction coefficient $\bar{A}_s = V_oA_s$

camber coefficient $\bar{A}_\gamma = L A_\gamma$

In the following and in the computer circuits the bars will be omitted.

NON-DIMENSIONAL EQUATIONS

For the flexible carcass model we obtain the following equations (bars omitted):

50

$$m \, \alpha_T^2 \, \ddot{v} + c_y \, \alpha_T \, \dot{v} + k_y v = q_y$$

$$m \, \alpha_T^2 \, \ddot{u} + c_x \, \alpha_T \, \dot{u} + k_x u = q_x$$

$$q_x = - \, q_H \, V_{sx}/V_s \quad , \quad q_y = - \, q_H \, V_{sy}/V_s$$

$$q_H = \mu \, q_z \qquad , \quad q_z = q_z(x)$$

$$\mu = \mu \, (V_s) = \mu_0 (1 - A_s V_s) \text{ or } = \mu_0 (1 - A_s V_s + B_s V_s^2)$$

$$V_s = \sqrt{V_{sx}^2 + V_{sy}^2}$$

$$V_{sx} = V_{cx} + \alpha_T \, \dot{u}$$

$$V_{sy} = V_{cy} + \alpha_T \, \dot{v} - V_r \left(\frac{dv_c}{dx} + A_\gamma \dot{\gamma} x \right)$$

$$V_x = V \cos \alpha$$

$$V_{cy} = V \sin \alpha$$

$$V_{cx} = s_x V_x$$

$$V_r = V_x - V_{cx}$$

$$x = 0.5 - V_r t/\alpha_T \quad \begin{cases} \leq 0.5 \\ \geq -0.5 \end{cases}$$

$$t = T - (i-1)\Delta T$$

$$\Delta T = \alpha_T/V_r$$

$$\Delta x = 1/N$$

$$x_k = 0.5 - k\,\Delta x \qquad k = 1,2,\ldots,N$$

$$q'_y = c_y\,\alpha_T\,\dot{v} + k_y\,v$$

$$q'_x = c_x\,\alpha_T\,\dot{u} + k_x\,u$$

MEMORY ARRAY M

at $x = x_{k-1}$ (start of step k):

$$q'_{y_{i-1,\ k-1}} = M(N)$$

$$q'_{y_{i-1,\ k-1}} = M(N-1)$$

shift of array

$$M(1) = q'_{y_{i,k-1}} = q'_y$$

$$g = N(q'_{y_{i-1, k}} - q'_{y_{i-1, k-1}})$$

$$q'_{y_{i-1}} = q'_{y_{i-1, k-1}} + g(x_{k-1} - x)$$

$$\Delta q'_y = q'_y - q'_{y_{i-1}}$$

$$v_{cj} = \frac{V_r}{\alpha_T} \int_0^T G_i(x) \, \Delta q'_y(x) \, dt + v_{cj_{i-1}} \qquad j = 1,2$$

parabolic interpolation with tangent relation at $x = 0.5$

$$\tilde{v}_c = \beta_y(a_0 + a_1 \xi + a_2 \xi^2)$$

$$a_0 = (3v_{c1} + v_{c1}/\sigma + v_{c2})/4$$

$$a_1 = v_{c1} - v_{c2}$$

$$a_2 = -v_{c1} - v_{c1}/\sigma + v_{c2}$$

at $\xi = x$:

$$\frac{dv_c}{dx} = a_1 + 2a_2 x - G(x,x)\Delta q'_y$$

$$\tilde{u}_c = \beta_x F_x/K_x$$

$$F_x = F_{x_{i-1}}$$

$$\int_0^t dF_x = \frac{V_r}{\alpha_T} \int_0^t q'_x(x) dt$$

$$F_y = \frac{V_r}{\alpha_T} \int_0^t \Delta q'_y(x) dt + F_{y_{i-1}}$$

$$M_z = M_{z_{i-1}}$$

$$\int_0^t dM_z = \frac{V_r}{\alpha_T} \int_0^t \{(x + \tilde{u}_c + u) \, q'_y(x) - (\tilde{v}_c + v) \, q'_x(x)\} dt$$

at $x = -0.5$ (end of run i):

$$v_{c1_i} = v_{c1} \quad , \quad V_{c2_i} = v_{c2}$$

$$F_{x_i} = \int_0^t dF_x \quad , \quad F_{y_i} = F_y \quad , \quad M_{z_i} = \int_0^t dM_z$$

APPENDIX III

DIGITAL PROGRAMS, ANALOG AND LOGIC CIRCUITS

The listing of the digital computer program for the rigid carcass model is presented on page 57 and 58. It contains a DO-loop which automatically provides a matrix of input values. This is accomplished by entering 1 on the keyboard. By entering 2 another portion of the program is followed which makes use of input values set by the potentiometers and read by the ADC's. Entering 3 results in exit from the computer. The analog and logic circuits are given in Figures 19 and 20.

The listing for the flexible carcass model is given on pages 61, 62, and 63. The program provides for a sweep in α. The slip angle starts at the value given by potentiometer 007. The slip angle α will be incremented with $3°$ after NN runs have taken place at constant α. The new series of runs starts with the carcass deflections found at the end of the previous series. The number NN has been taken large enough in order to attain steady-state for each α-value. The value of NN is taken smaller for larger α. After the maximum of $20°$ the slip angle drops each time with $3.01°$. After a series of runs for a certain α has started, the switches in the analog circuit (Fig. 16) are in position A (full lines) so that $\Delta q'_y$ is integrated. After each run the switches will be set in position B (dashed lines). This

is controlled by the digital computer with the control line register (= M1(=1) when in A and =M2(=0) when in B). After omitting the framed portions indicated in the program, the version without the sweep is obtained. Statement 80 gives the probability to stop the series of runs. When sense line 4 is high, the series is stopped, the output is printed and new input values may be entered (after statement 8). Statement CALL TSCAL(L,1) causes the system (except integrators 310, 320 and 330, see logic diagram) to speed up with a factor ten. The flow diagram of Figure 10 may clarify the digital program. Note: Figure 10 does not include the sweep and the switches.

Figures 21 and 22 present the complete analog and logic circuit for the flexible tire model. The simplified versions shown in parts in Figures 4, 5 and 9 clarify the course of computations.

```
// JOB           ?    ?    20 DEC 71 11.663 HRS
// FOR NM001    20 DEC 71 11.663 HRS
*ONE WORD INTEGERS
*IOCS(TYPEWRITER,KEYBOARD)
*LIST SOURCE PROGRAM
**       MOVING TREAD ELEMENT TIRE MODEL WITH RIGID CARACASS
```

```
        DIMENSION ALFA(5), SX(6), IFO(4), LFO(4), ISO(3), LSO(3),
       2 LSI(3), LFI(3)
        DATA   ALFA/ 0., 2., 4., 8., 16./
        DATA   SX/ 0., .025, .05, .075, .1, .25/
        DATA   ISO/1153, 1155, 1157/
        DATA   IFO/1152,1154,1156,1158/
        DATA   ISI/3216/
        DATA   IFI/3248/
        CALL  HYBON
        CALL  NOTST(1,3)
        CALL  INITA(L,0)
        CALL  RUN(L)
        CALL  TSCAL(L,1)
     10 CALL  IC(L)
        CALL  SENSW(0,L)
        WRITE(15,1000)
        READ(17,3000)IGO
        GO TO (20,30,40),IGO
     20 V=.5
        DO 80 I=1,5
        ALF=3.1416*ALFA(I)/180.
        VX=V*COS(ALF)
        VCY=V*SIN(ALF)
        DO 80 J=1,6
        VCX=SX(J)*VX
        VR=VX-VCX
        LSO(1)=VCX*10000.
        LSO(2)=VCY*10000.
        LSO(3)=VR*1000.
        CALL  STBLK(ISO,LSO,3)
        LFO(1)=VR*1000.
        LFO(2)=VR*1000.
        LFO(3)=VR*1000.
        LFO(4)=VR*1000.
        CALL  STBLK(IFO,LFO,4)
        CALL  OP(L)
     50 IF (ITEST(L,0,4)) 60,60,10
     60 IF (ITEST(L,0,1)) 50,50,70
     70 CALL  HOLD(L)
        CALL  SCANH(IFI,LFI,3)
        FX=LFI(1)/10000.
        FY=LFI(2)/10000.
        XMZ=LFI(3)/10000.
        CALL  IC(L)
```

57

```
      CALL SENSW(0,L)
      WRITE(15,2000)ALFA(I),SX(J),FX,FY,XMZ
      WRITE(15,4000)
      READ(17,3000)IPO
   80 CONTINUE
      GO TO 10
   30 CALL SCANH(ISI,LSI,3)
      V=LSI(1)/10000.
      ALFAI=LSI(2)/100.
      SXI=LSI(3)/10000.
      ALF=3.1416*ALFAI/180.
      VX=V*COS(ALF)
      VCY=V*SIN(ALF)
      VCX=SXI*VX
      VR=VX-VCX
      LSO(1)=VCX*10000.
      LSO(2)=VCY*10000.
      LSO(3)=VR*1000.
      CALL STBLK(ISO,LSO,3)
      LFO(1)=VR*1000.
      LFO(2)=VR*1000.
      LFO(3)=VR*1000.
      LFO(4)=VR*1000.
      CALL STBLK(IFO,LFO,4)
      CALL OP(L)
   90 IF (ITEST(L,0,4)) 100,100,10
  100 IF (ITEST(L,0,1)) 90,90,110
  110 CALL HOLD(L)
      CALL SCANH(IFI,LFI,3)
      FX=LFI(1)/10000.
      FY=LFI(2)/10000.
      XMZ=LFI(3)/10000.
      CALL IC(L)
      WRITE(15,2000)ALFAI,SXI,FX,FY,XMZ
      GO TO 10
   40 CALL IC(L)
      CALL LOAD(L)
      CALL HOFF(L,0)
      CALL EXIT
 1000 FORMAT(/'ENTER 1, 2 OR 3')
 2000 FORMAT(/' ALPHA = ',F6.2,' SX = ',F6.2/' FX = ',F8.4,' FY = ',
     2  F8.4,' MZ = ',F8.5)
 3000 FORMAT(I1)
 4000 FORMAT(/'XXXXXXXXXX')
      END
```
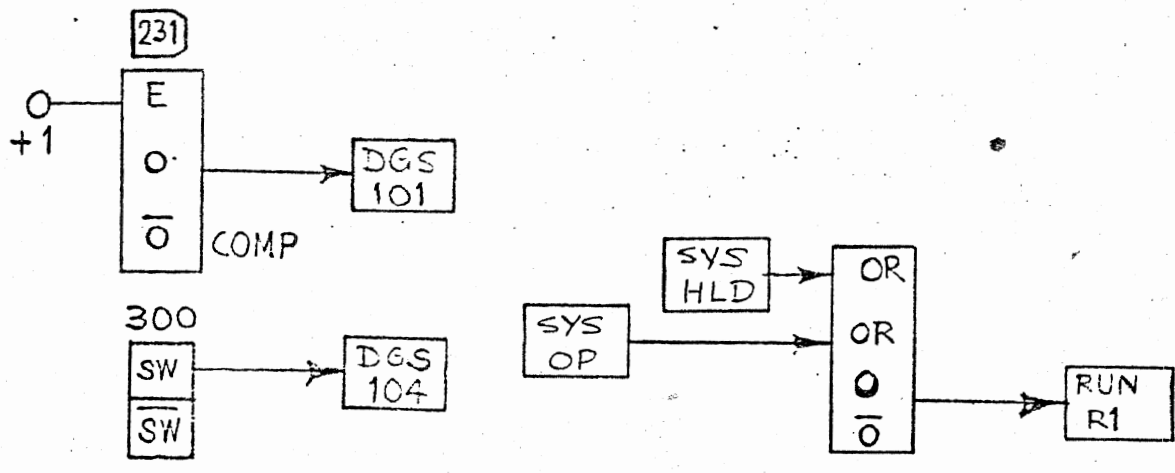
Figure 19. Analog circuit for rigid carcass model

Figure 20. Logic circuit for rigid carcass model

// JOB   ?   ?   18 OCT 71. 11.373 HRS
// FOR HP001   18 OCT 71 11.373 HRS
*ONE WORD INTEGERS
*IOCS(TYPEWRITER,KEYBOARD)
*LIST SOURCE PROGRAM
** HP001 MOVING TREAD ELEMENT TIRE MODEL WITH FLEXIBLE CARCASS

```
       DIMENSION M(20),P(20),          LSI(4),IOU(6),LSO(6),LFI(7),
      +LFO(6),IOO(3),LOO(3),IFO(6)
       DATA IFO/1158,1159,1160,1161,1162,1163/
       DATA IIN/3216/
       DATA IOU/1153,1155,1152,1154,1156,1157/
       DATA IOO/1164,1165,1166/
       DATA IFI/3280/
       DATA IOI/3250/
       DATA IXK/1166/
       DATA IVR/1167/
       N=20
       NO=16
       TOL=10.
       DX=1./N
       ALFT=1.
       AG=.7
       M1=1
       M2=0
    8  CALL IC(L)
       WRITE(15,1000)
 1000  FORMAT(/'ENTER 1 TO EXECUTE',/,'ENTER 2 TO EXIT')
       READ(17,2000) IGO
 2000  FORMAT(I1)
       GO TO(9,300),IGO
    9  CALL HYBON
       CALL NOTST(1,3)
       CALL INITA(L,0)
       CALL RUN(L)
       CALL TSCAL(L,1)
       CALL SCANH(   IIN ,LSI,4)
       LL=0
       DO 40 J=1,6
   40  LFO(J)=0
       ALPHA=LSI(2)/100.
       DO 50 J=1,20
   50  M(J)=0
 2500  CALL STBLK (IFO,LFO,6)
       NO= 16.*(1.-ALPHA/20.)*(1.-ALPHA/20.)*(1.-ALPHA/20.)
       LXK=5000
       XK=.5
       V=LSI(1)/10000.
       ALF=3.1416*ALPHA/180.
       SX=LSI(3)/10000.
       GAMMA=LSI(4)/100.
       VX=V*COS(ALF)
```

61

```
      VCY=V*SIN(ALF)
      VCX=SX*VX
      VR=VX-VCX
      VRAT=VR/ALFT
      LSO(1)=VCX*10000.
      LSO(2)=VCY*10000.
      LSO(3)=AG*GAMMA*10000.*3.1416/180.
      LSO(4)=VR*10000.
      LSO(5)=VRAT*10000.
      LSO(6)=VRAT*1000.
      LVR=VRAT*10000.
      LFI(5)=0
      CALL STBLK(  IOU ,LSO,6)
      CALL STINH(IXK,LXK)
      CALL STINH (IVR,LVR)
      M(N)=0
      CALL READH(IQI,IQK)
      CALL IC(L)
      K=1
      CALL SETWD (0,MI)
      KL=1
      GO TO 210
  80  IF(ITEST(L,0,4)) 85,85,800
  85  IF (ITEST(L,0,1)) 90,90,100
  90  IF (ITEST(L,0,2)) 80,80,200
 100  CALL HOLD(L)
      FY=LFI(5)
      CALL SCANH (IFI,LFI,7)
      LFO(1)=LFI(1)
      LFO(2)=LFI(2)
      LFO(3)=LFI(3)
      TEMP=LFI(4)
      LFO(4)=VRAT*TEMP
      LFO(5)=LFI(5)
      TEMP=LFI(6)
      LFO(6)=VRAT*TEMP
      NN=NO*VR/VX+5 + 1000 -1000
      IF(NN-K) 101,101,110
 101  VC1=LFO(1)/10000.
      VCO=LFO(2)/10000.
      VC2=LFO(3)/10000.
      FX=LFO(4)/1000.
      FY=LFO(5)/10000.
      XMZ=LFO(6)/10000.
      FZ=LFI(7)*VRAT/1000.
      IF(ALPHA-1.) 999,900,900
 900  IF(LL-0) 901,901,906
 901  IF(ALPHA-20.) 902,906,906
 902  ALPHA=ALPHA+3.
      GO TO 2500
 906  ALPHA=ALPHA-3.01
      LL=1
      GO TO 2500
 999  GO TO 8
 110  CALL STBLK (IFO,LFO,6)
      XK=0.5
```
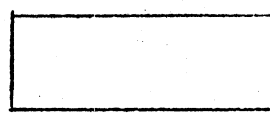
omit when no
sweep desired

```
      K=K+1
      IF (KL)120,119,120
119   CALL SETWD (0,M1)
120   IF (KL-4)122,121,121
121   CALL SETWD (0,M2)
      KL=0
      GO TO 124
122   L1=NN-1
      IF (L1-K)121,121,123
123   KL=KL+1
124   M(N)=0
      CALL READH (IQI,IQK)
      CALL IC (L)
      GO TO 210
200   CALL HOLD (L)
      CALL READH (IQI,IQK)
210   LG=2*(M(N-1)-M(N))
      LH=M(N)
      DO 220 J=1,19
      KK=21-J
220   M(KK)=M(KK-1)
      M(1)=IQK
      XK=XK-DX
      LXK=10000.*XK
      LQO(1)=LG
      LQO(2)=LH
      LQO(3)=LXK
      CALL STBLK (IQO,LQO,3)
      CALL SENSW (0,MM)
      CALL OP (L)
      GO TO 80
800   WRITE(15,103)V,ALPHA,SX,GAMMA,K,FZ
      DO 102 J=1,20
102   P(J)=M(J)/10000.
103   FORMAT(/'V=',F6.2,' ALPHA=',F6.2,' SX=',F6.2,' GAM=',F6.2,' K=',
     +I5,' FZ=',F8.4)
105   FORMAT(/' FX=',F8.4,'   FY=',F8.4,' XMZ=',F8.5)
      WRITE(15,105)FX,FY,XMZ
      GO TO 8
300   CALL IC (L)
      CALL LOAD (L)
      CALL HOFF (L,0)
      CALL EXIT
      END
```
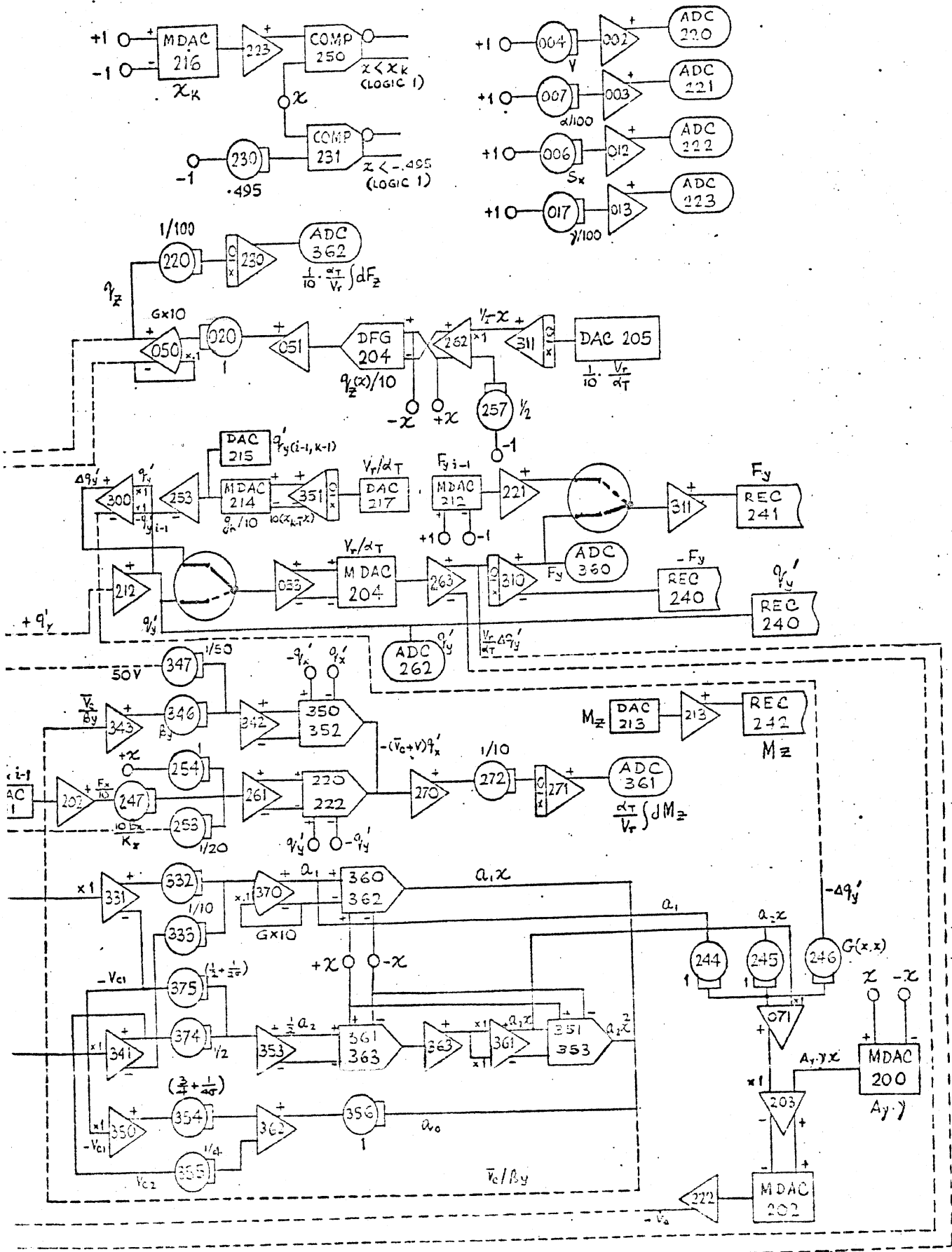
Figure 21a. Portion of analog circuit for flexible carcass tire model
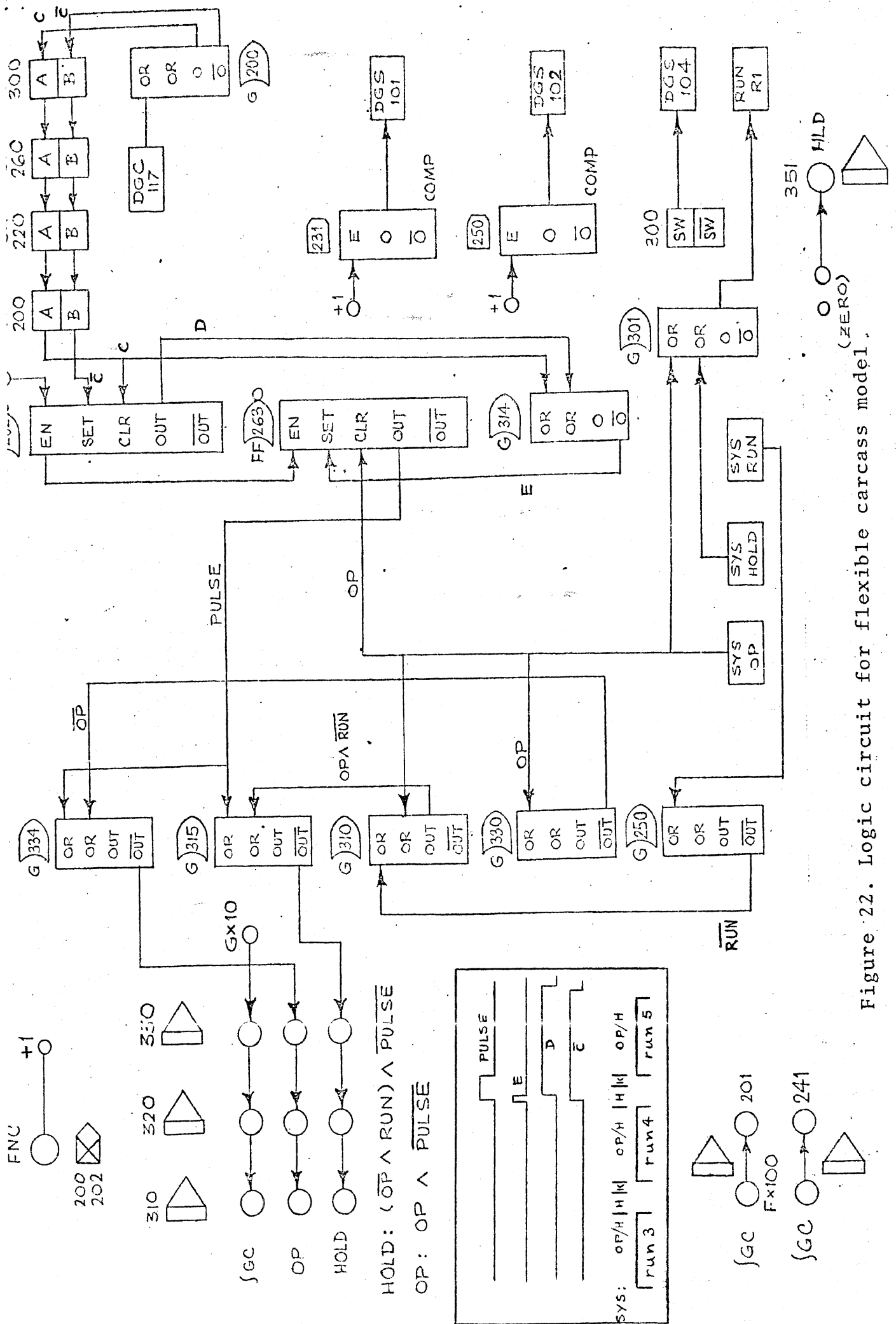
64

Figure 22. Logic circuit for flexible carcass model.

APPENDIX IV

FUNCTIONS AND PARAMETERS

The vertical pressure distribution, $\bar{q}_z$, friction coefficient functions, and the Green functions, $\bar{G}$, which have been used in the analysis are shown in Figures 23, 24, and 25. The parameter and potentiometer values are listed in Table 1.
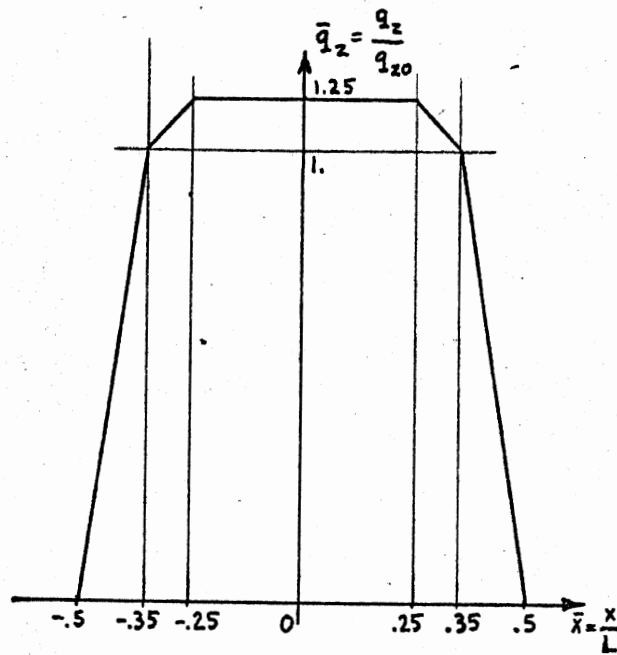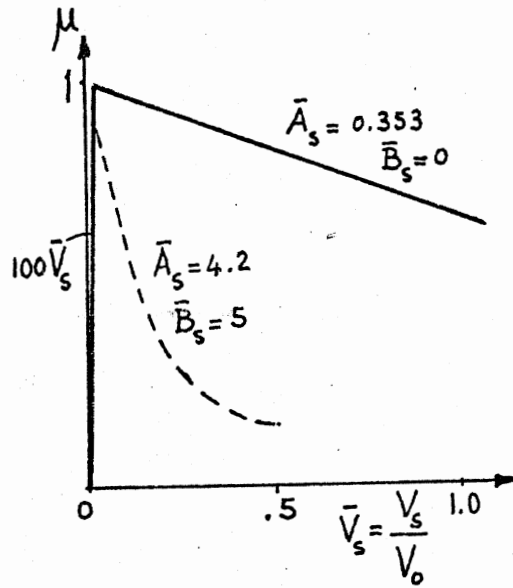

Figure 23. Pressure distribution
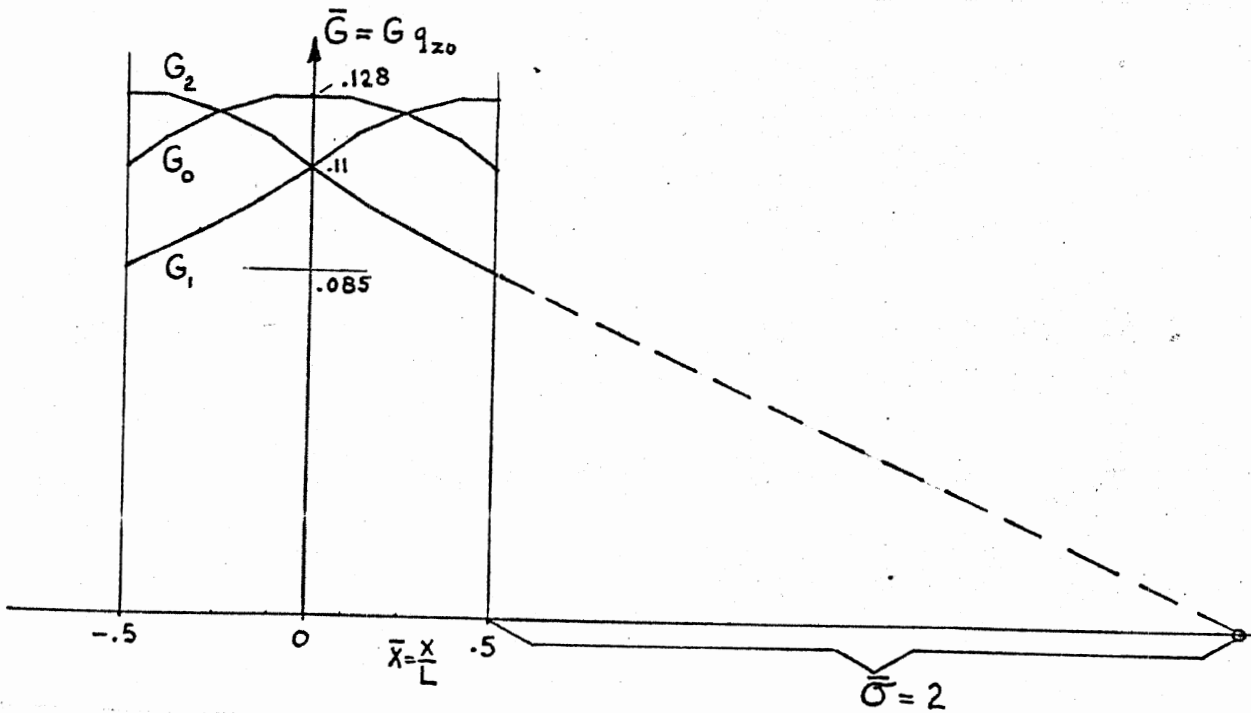
Figure 24. Coefficient of friction

Figure 25. Green functions

TABLE 1

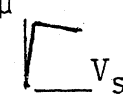| NON-DIMENSIONAL COEFFICIENT	POT. NO.	ALL CASES	PARAMETER VALUES			REMARKS
			FLEXIBLE CARCASS		RIGID CARCASS	
			$\mu\, \sqsubset\!\_V_s$	$\mu\, \wedge\!\_V_s$	$\mu\, \sqsubset\!\_V_s$	
V	004					
s_x	006					
$\alpha/100$	007					
	013	1.0				
	014	1.0				
$A_s \mu_o/10$	015		0.0353	0.42	0.0353	
$\gamma/100$	017					
	020	1.0				
$\mu_o/10$	022	0.1				
	024	1.0				
$B_s \mu_o/10$	025		0.0	0.5	0.0	
	026	0.1				
	027		0.1	0.1	0.2	
	220	0.01				
$1/(10\ m\ \alpha_T)$	222		1.0	1.0	0.5*	$1/(20\ m\ \alpha_T)$
$1/(2\ \alpha_T)$	223	0.5				
$k_y/50$	226		0.8	0.8	1.0*	$k_y/25$
$c_y/10$	227		0.3	0.6	0.3*	$c_y/5$
	230	0.495				

TABLE 1 (Continued)

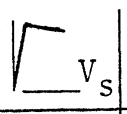| NON-DIMENSIONAL COEFFICIENT	POT. NO.	ALL CASES	FLEXIBLE CARCASS $\mu\,\llcorner\!\!\!\!\!\_ V_s$	FLEXIBLE CARCASS $\mu\,\lfloor\!\!\backslash\!\!\_ V_s$	RIGID CARCASS $\mu\,\llcorner\!\!\!\!\!\_ V_s$	REMARKS
$1/(10\ m\ \alpha_T)$	232	1.0				
$1/(5\ \alpha_T)$	233	0.2				
$k_x/20$	234	1.0				
$c_x/10$	235		0.2	0.6	0.2	
	242	0.01			-	
	244	1.0			-	
	245	1.0			-	
$G(x,x)$	246		0.128	0.05*	-	More stable
$10\beta_x/K_x$	247	0.227		-	-	
	253	0.05				
	254	1.0				
	257	0.5				
	272	0.1			-	
	316	1.0			-	
	322	0.1			-	
	324	0.1			-	
	327	1.0			-	
	332	0.1			-	
	333	0.1			-	
β_y	346	0.8				
	347		0.02	0.02	0.04	

TABLE 1 (Continued)
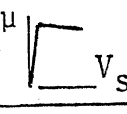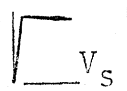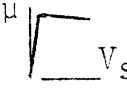
NON-DIMENSIONAL COEFFICIENT	POT. NO.	PARAMETER VALUES				REMARKS
		ALL CASES	FLEXIBLE CARCASS μ ⌐ V$_s$	μ Λ V$_s$	RIGID CARCASS μ ⌐ V$_s$	
$\beta_x/K_x - \beta_y/K_y$	350		-	-	0.04	
$(3 + 1/\sigma)/4$	354	0.875			-	
	355	0.25			-	
	356	1.0			-	
	374	0.5			-	
$(1 + 1/\sigma)/2$	375	0.75			-	